Tectonophysics 602 (2013) 106–123

Contents lists available at SciVerse ScienceDirect

Tectonophysics

journal homepage: www.elsevier.com/locate/tecto

# Surface topography as key constraint on thermo-rheological structure of stable cratons

Thomas François *, Evgueni Burov, Bertrand Meyer, Philippe Agard

*UPMC Univ Paris 06, ISTEP UMR 7193, Université Pierre et Marie Curie, F-75005, Paris, France*
*CNRS, ISTEP, UMR 7193, F-75005, Paris, France*

ARTICLE INFO

*Article history:*
Received 17 February 2012
Received in revised form 7 September 2012
Accepted 3 October 2012
Available online 13 October 2012

*Keywords:*
Craton
Lithosphere
Topography
Rheology
Plate tectonics

ABSTRACT

Why some Archean cratons survived for billions of years while the rest of the lithosphere has been reworked, probably for several times, is both enigmatic and fundamental for plate tectonics. Craton longetivity is mainly explained by their buoyancy and analyzed by testing gravitational stability of hardly detectable cratonic mantle "keels" as a function of a hypothesized thermo-rheological structure. Destruction of some cratons suggests that buoyancy is not the only factor of their stability, and many previous studies show that their mechanical strength is equally important. The upper bounds on the integrated strength of cratons are provided by flexural studies demonstrating that $T_e$ values (equivalent elastic thickness) in cratons are highest in the world (110–150 km). Yet, the lower bounds on the integrated strength of stable cratons are still a matter of debate, as well as the question on how this strength is partitioned between crust and mantle, and which set of rheological parameters is most pertinent. We show that primary observed cratonic features – flat topography and "frozen" heterogeneous crustal structure – represent the missing constraints for understanding of craton longevity. The cratonic crust is characterized by isostatically misbalanced density heterogeneities, suggesting that the lithosphere has to be strong enough to keep them frozen through time without developing major gravitational instabilities and topographic undulations. Hence, to constrain thermo-rheological properties of cratons one should investigate the stability of their topography and internal structure. Our free-surface thermo-mechanical numerical models demonstrate that craton stability cannot be warranted even by very high crustal strength, so that dry olivine mantle and cold thick lithosphere are indispensable conditions. We establish lower-bound limits on the thermo-rheological structure of cratons. In particular, we find that minimal $T_e$ needed for long-term stability of continents is approximately 90–110 km of which at least 70 km should be "contributed" by the lithosphere mantle.



## 1. Introduction

Preservation of Archean cratons for billions of years remains one of the fundamental problems of geodynamics since the emergence of the plate tectonics paradigm (Fig. 1). Since their formation, cratons have moved all around the Earth's surface but remained largely intact (e.g., Griffin et al., 2003), surviving multiple plate reorganizations that led to destruction or essential reworking of the rest of the lithosphere. Phenomena leading to recycling of non-cratonic and cratonic lithosphere and related mantle–lithosphere interactions have been treated in a great number of geodynamic modeling and analytical studies (e.g., Bird, 1979; Houseman and Molnar, 1997; Pysklywec et al., 2000; Rowland and Davies, 1999; Sleep, 2003a,b,c; Tao and O'Connell, 1992; Willet et al., 1993). The mechanisms of craton survival have attracted as much attention (e.g., Beuchert et al., 2010; Lenardic et al., 2003; Sleep, 2003b), yet there is still no consensus on which factors play major role here: crustal or mantle compositional buoyancy, rheological strength of the lithospheric mantle or that of the lithospheric crust. The Canadian and Australian cratons represent emblematic examples of stable cratons, probably due to the lack of major asthenospheric perturbations. Cratonic lithosphere can nevertheless be fragmented by plume events and major thermal events, such as few cases of Proterozoic and Phanerozoic thermal rejuvenation (e.g., Gamburtsev Mountain Range, Ferraccioli et al., 2011), or marginally destroyed on its edges due to lateral heat exchanges and density gradients (e.g., North China craton: Bleeker, 2003; Griffin et al., 2003; Xu, 2001). Cratons also attract growing attention of the geodynamic community for understanding the dynamics of the Early Earth and terrestrial planets and because they represent key proxies for the much debated, long-term rheological and thermal properties of the lithosphere (i.e., end-member rheological concepts such as the "Crème Brûlée" and "Jelly Sandwich" models; Burov and Watts, 2006; Jackson, 2002; see below).

Although the mechanisms of cratonic survival are still debated, it is generally agreed that their stability must relate to their differences from "ordinary" platform lithosphere. We herein follow the broad

* Corresponding author. Tel.: +33 11 44 27 59 43.
*E-mail address:* thomas.francois@upmc.fr (T. François).

0040-1951/$ – see front matter © 2012 Elsevier B.V. All rights reserved.
http://dx.doi.org/10.1016/j.tecto.2012.10.009

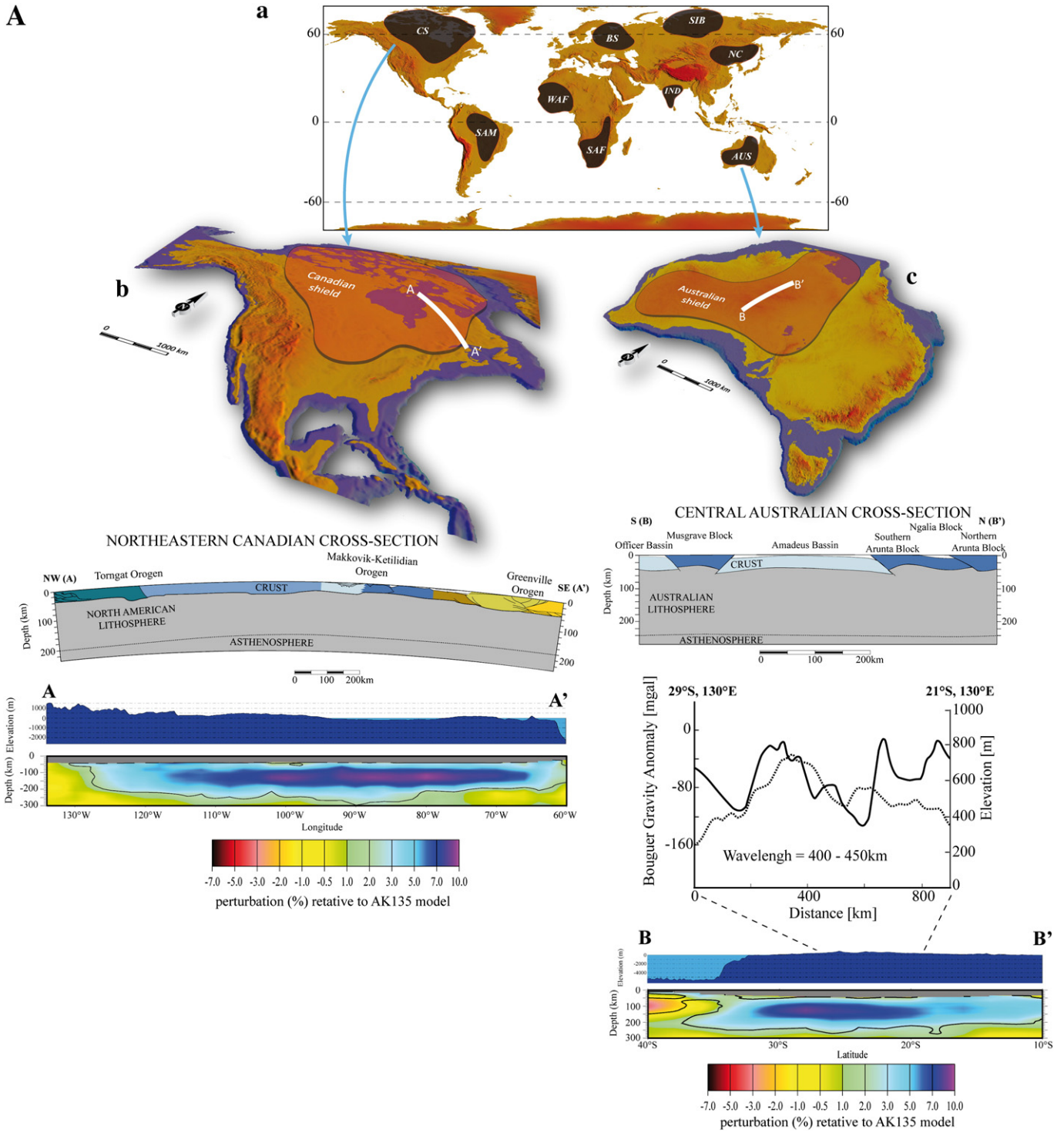


**Fig. 1.** A: Archean regions of the world. a Worldwide distribution of cratonic terrains with a zoom onto two well-preserved Archean cratons, the Canadian Shield b and the Australian Shield c. Legend: CS, Canadian shield; AUS, Western Australia; BS, Baltic shield and East European Platform; NC, North China shield; SAM, South American craton; SIB, Siberian Platform; SAF, South African craton; and WAF, West African craton. b Canadian shield and location of the lithospheric cross-section "Northeastern lithospheric profile", AA′ based on the data of the LITHOPROBE project (modified from Hammer et al., 2010). c Australian shield and location of the lithospheric cross-section "Central Lithospheric Profile", BB′ (after Clitheroe et al., 2000; Ford et al., 2010; Stephenson and Lambeck, 1985). Note the highly heterogeneous inherited crustal structure in both cases. Shown also are surface topography of the Australian craton and the associated Bouguer gravity anomaly (after Lambeck, 1986) witnessing periodic anomalies associated with whole-scale lithospheric folding. The bottom inserts present surface shear wave tomography (CUB) anomalies extracted from the model of N. Shapiro (http://ciei.colorado.edu/~nshapiro/MODEL/, Shapiro et al., 2002). B: Alternative thermal models for cratons, matched to the mantle xenolith data. As can be seen, large scatter in data derived from different sources does not allow inferring discriminating constraints on mantle lithosphere geotherms from xenolith data only, even though some local data (e.g., Kopylova et al., 1999) show a good internal consistency. The largely missing parameter is the thermal thickness of the lithosphere, i.e. the depth to 1330 °C. C: Left: typical model for testing stability of "normal" lithosphere with undepleted negatively buoyant mantle, with rigid-top upper boundary condition that neglects surface evolution. Right: In case of negatively buoyant mantle, RT instabilities develop in mantle roots (LAB) leading to gravitational collapse and deblobbing of the mantle lithosphere (after Burov and Watts, 2006). This approach is generally based on the analytical models of RT instability and allows for discrimination between different thermo-rheological assumptions for heavy undepleted lithospheres. However, in case of positively buoyant depleted mantle RT instabilities will not develop, at least in analytical models or in numerical models without strong perturbations leading to convective instabilities. Also LAB is hard to detect to match the observations with nature. Hence this method is not efficient for cratons.

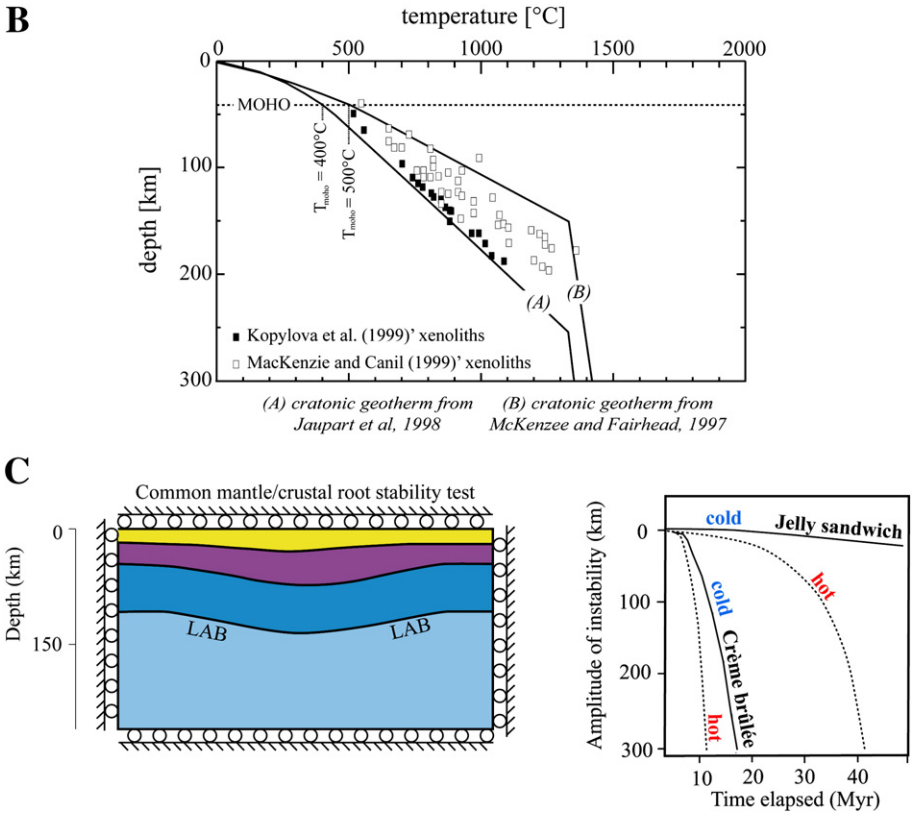


**Fig. 1** (*continued*).

understanding that stable cratons refer to vast continental areas with rocks >2.5 Ga having remained mostly undeformed since then, with generally smooth internal topography, low heat flux and thick lithosphere. More specifically, the following features also discriminate cratons (we cite here not only data sources but also modeling studies concerned with particular characteristics of cratons): (a) great seismic thickness ($H_s$, ~200–350 km) defined as a region of distinctly faster than average seismic velocities (by 1.5–2%) in global *S* velocity tomographic models (Cooper and Conrad, 2009; Gung et al., 2003; Sleep, 2003b), or depth of lithosphere–asthenosphere boundary (LAB); (b) positive buoyancy of the cratonic mantle associated with chemical depletion (Doin et al., 1997; Jordan, 1981; Poudjom Djomani et al., 2001; Shapiro et al., 1999); (c) low surface heat flux (30–50 mW/m$^2$) (Lévy and Jaupart, 2011; Lévy et al., 2010; Mareschal and Jaupart, 2004), which is generally interpreted as a consequence of their important thermal thickness, $H_t$, but also of low internal heat production; and (d) high integrated mechanical strength, revealed by flexural isostasy studies (Audet and Bürgmann, 2011; McKenzie and Fairhead, 1997; Watts, 2001) and generally explained by cold mantle geotherm and depletion of water (dry rheology).

Several reasons nevertheless call for a thorough reinvestigation of the stability of cratons:

(1) Although positive buoyancy and high mechanical strength (Cooper and Conrad, 2009; Sleep, 2003b) have so far been regarded as the prevalent conditions for cratonic and more generally lithospheric stability, the respective contributions of crust and mantle to the integrated strength, and hence stability, of cratons is unknown.

(2) The common approach to lithosphere stability is to test different thermal and simplified rheological assumptions in terms of their impact on the growth rates of gravitational thermo-mechanical instabilities at the lithosphere–asthenosphere boundary (LAB) (Fig. 1C). However, the LAB itself is not the best reference because its depth, nature, and geometry are strongly debated (e.g., Artemieva, 2009; Eaton et al., 2009; Fischer et al., 2010; Karato, 2012).

(3) One key characteristic of cratons has so far been neglected: the central zones of cratons generally have a smooth topography, which remained largely unchanged (Belton et al., 2004 and references therein; Pillans, 2007; Stewart et al., 1986), sometimes over very long periods of time (>200 Myr), and show little correlation with known subsurface loads. This is, for example, attested in the Canadian and Australian craton by the very little amount of sedimentation or erosion of intra-cratonic origin. Overall, sedimentation/erosion of intra-cratonic origin appears to be very low (<2.5 μm/yr in average since ca. 1.7 Ga; Flowers et al., 2006) and in many areas Precambrian rocks croup out at the surface. Within the Australian craton, denudation rates are also negligibly low, in the range 0–2 m/Myr since the Mesozoic (Belton et al., 2004; Bierman and Caffee, 2002; Gale, 1992). It must nevertheless be acknowledged that, in a number of cases, the topographic stability of cratons has been perturbed by external tectonic and mantle dynamic events. Examples include the recent Arctic cordilleran folding and faulting (1.5 km high Torngat Mountains of the Nain Craton; Hammer et al., 2010), the break-up of Gondwana some 150 Ma (Western Ghats still culminating at 2650 m above sea level in the Dharwar craton; Gunnell and Fleitout, 2000) or the large-scale plume-related dynamic topography of the 1.5 km high Kaapvaal craton (South Africa, Gurnis et al., 2000). However, in the absence of major thermal events or external forcing, as for the central regions of the Canadian and Australian cratons, the topography of the cratonic lithosphere seems to be very stable over >200 Myr, and, importantly, insensitive to the presence of buried crustal loads inherited from previous tectonic history.

We thus herein explore the idea that the sensitivity of the surface topography to the internal loads should help further characterize their rheological strength and stability. We also take a straightforward yet unprecedented approach using the geometries of the only well-constrained interfaces, surface topography and Moho. Tracking the evolution of topography is indeed now permitted by a new generation of thermo-mechanical models that implement free-surface boundary conditions, allowing us to analyze variations of surface (>10 m) and Moho topography, in addition to that of the LAB. The second novelty for lithosphere stability analysis lies in the implementation of a petrologically-consistent density structure (computed from the thermodynamic code Perple_X) and explicit viscous (ductile)–elastic–plastic (brittle) rheology laws in large-strain numerical formulation, instead of more common viscous or viscous–pseudoplastic rheologies (Lenardic et al., 2003) or visco-elastic rheologies (Beuchert et al., 2010). The first set of experiments shown here explores the conditions of the stagnant lid approximation (i.e., flat layered homogeneous lithosphere structure in the absence of far-field forces). The second and third sets explore the implications of a laterally heterogeneous crustal structure without or with tectonic compression, respectively, with reference to the Canadian and Australian cratons, which are likely to have preserved the rheological profile of stable cratonic lithosphere. Our aim is to reproduce the overall characteristics of these cratons rather than every single detail. The robustness and significance of our results are then discussed, with emphasis on their rheological implications.

## 2. Methodology

### 2.1. Possible rheological assumptions

The rheology and strength of the Earth's lithosphere have been a topic of debate ever since the beginning of the 20th century, when Joseph Barrell introduced the concept of a strong lithosphere overlying a fluid asthenosphere (e.g. Watts, 2001; Watts and Burov, 2003 and references therein). The question of how the strength of the plates varies spatially and temporally is fundamental to geology and plate tectonics (e.g., Burov, 2010; Burov and Watts, 2006; Jackson, 2002).

The main proxy to the integrated long-term strength of the lithosphere is its equivalent elastic thickness, $T_e$, derived from studies of flexural isostasy. This integrated strength of continental plates varies within large limits (Audet and Bürgmann, 2011; Watts, 2001 and references therein), highlighting cratons as the strongest lithospheric blocs in the world. $T_e$ is generally highest in coldest plates (characterized by lowest surface heat flow), reflecting the fact that thermal structure of the lithosphere primarily controls its rheological strength profile (Burov, 2011 and references therein; Fig. 2A).

The rheological interpretation of flexural observations is not straightforward, however, since it requires additional constraints on rheological parameters of at least one of the major structural units (i.e., crust or mantle; Burov, 2011). For any given rock mineralogical composition and microstructure, the most important controlling parameters are temperature, fluid content, pressure, strain, strain rate, strain history, grain size, fugacities of volatiles, and chemical activities of mineral components (Bürgmann and Dresen, 2008; Evans and Kohlstedt, 1995; Katayama et al., 2005; Keefner et al., 2011). Most of these parameters are poorly constrained in nature, unfortunately, explaining the difficulties of extrapolation of experimental rock mechanics data to geological conditions (Burov, 2011; Karato, 2010). These limitations have fuelled strong debates on the long-term strength of the lithosphere, including controversial evaluations of their thermal structure and equivalent elastic thickness $T_e$ (Burov, 2011; Watts and Burov, 2003).

Although it is agreed that measurable elastic thickness $T_e$ cannot be higher than 110–150 km (e.g., Audet and Bürgmann, 2011; Watts, 2001), there is neither agreement on the lower bounds of $T_e$ nor on the thermal thickness of the cratonic lithosphere ($H_t$; i.e., the depth at which T = 1330 °C) that controls its integrated strength (Artemieva, 2006; Artemieva and Mooney, 2001). Depending on assumptions on flexural models (specifically, for the two major antagonist approaches, based on Free Air gravity admittance and on Bouguer coherence), estimates for cratonic $T_e$ cluster either around values as low as 30–40 km (McKenzie ad Fairhead, 1997) or as high as 80–150 km implying, respectively, $H_t$ values ranging from 100–150 km to 250–300 km (Watts and Burov, 2003).

At the outcome, two opposite, end-member rheological concepts have emerged, namely the "Jelly Sandwich" and "Crème Brûlée" models (JS, CB; Fig. 2A) (Burov and Watts, 2006). In the JS model, the mantle lithosphere is strong and supports surface and buried tectonic loads, assuring mechanical and gravitational stability of the lithosphere, while the lower crust can be either strong or weak depending on its composition. The JS model is based on the assumption of a cold, thick thermal lithosphere and dry olivine mantle rheology (cold thermal conditions and absence of fluids both favor high rock strength). In the CB model, the lithospheric mantle is weak and strength is concentrated in the highly buoyant continental crust, which is supposed to keep afloat the entire lithosphere. This model assumes the hottest possible thermal structure and wet olivine mantle rheology (see also Fig. 1B).

### 2.2. Craton stability and stagnant lid approximation

The "normal" chemically undepleted mantle lithosphere is negatively buoyant, so that any perturbation of major density interfaces such as the LAB will result in Rayleigh–Tailor (RT) instabilities leading to lithospheric destruction by "de-blobbing" of the lithospheric mantle "keels" whose base may be identified with the LAB (Burov and Watts, 2006; Houseman and Molnar, 1997). Even in the case of a very strong (i.e., $T_e$ > 90–110 km; Burov and Watts, 2006) negatively buoyant mantle lithosphere, the development of RT instability takes a few hundred of millions of years at the most. This process cannot be slowed down to time scales larger than 300–400 Ma (Fig. 1C; Burov and Watts, 2006), and certainly not to time scales compatible with the lifespan of cratons, without reversing the density contrast between the lithosphere and asthenosphere. Positive buoyancy of cratonic mantle (Forte and Perry, 2000; Kopylova and Russell, 2000) is thus a key factor for the longevity of cratons.

Yet, even buoyant lithosphere may only be unconditionally stable under the "stagnant lid" condition (Solomatov, 1995; Solomatov and Moresi, 1997; 2000), i.e. when it has an infinite, horizontally homogeneous flat-layered structure not subjected to far-field tectonic forces, while the upper mantle convection parameters (such as the Rayleigh number) are tuned to prevent convective erosion of the LAB (see below). In nature, cratons are laterally heterogeneous, bordered by thinner "normal" lithosphere of contrasting density and may be subjected to far-field forces. If cratons were not strong enough, external forces, thermal and pressure gradients resulting from lateral variations in crustal thickness and density would result in significant perturbations of density and rheological interfaces (such as surface, LAB and Moho). Gravitational spreading, RT and marginal instabilities will develop at internal density interfaces, while the LAB may also be eroded by convective instabilities in the upper mantle (Guillou-Frottier and Jaupart, 1995; Korenaga and Jordan, 2002; Lenardic et al., 2003). The threshold of such perturbations therefore needs to be assessed.

### 2.3. Testing for two well-constrained natural case-examples: the Canadian and Australian cratons

As follows from the previous discussion, the Canadian and Australian shields (Fig. 1A) are "ideal" examples for testing lithospheric stability and its ability to preserve buried loads, specifically because in these well-preserved Archean cratons there is a host of available structural, thermal and other geophysical data allowing for the development of statistically representative structural and thermo-mechanical models. The

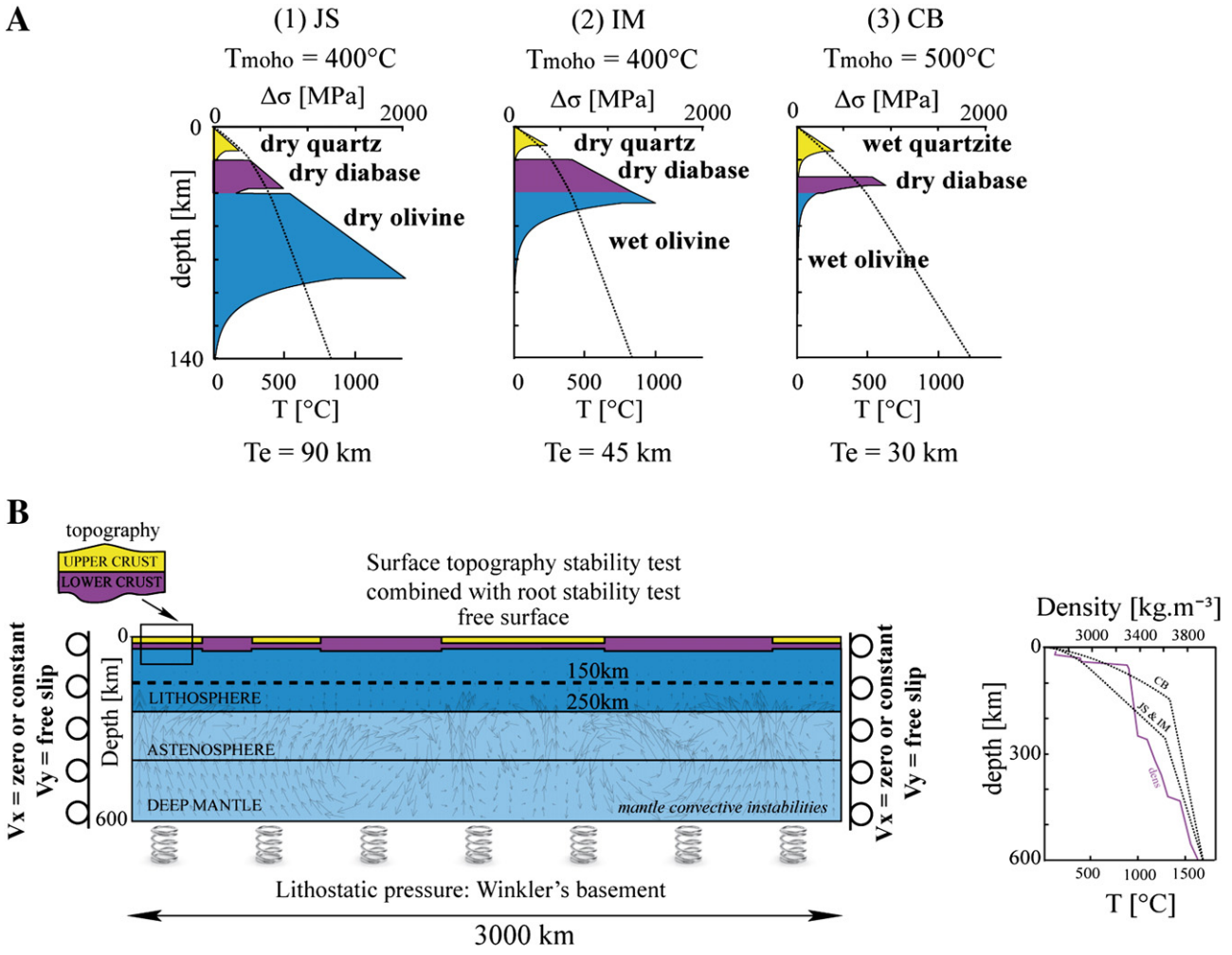


**Fig. 2.** A: Thermo-rheological profiles tested in the numerical experiments: two end-member assumptions (strongest and weakest rheology) and one intermediate case. Respectively: "Jelly Sandwich", JS, with dry olivine mantle part and 250 km thick thermal lithosphere ($H_t$) (Jaupart et al., 1998) (Moho temperature 400 °C); "Crème Brûlée" profile, CB, with weak wet olivine mantle part and 150 km thick thermal lithosphere ($H_t$) (Jackson, 2002) (Moho temperature 500 °C); Intermediate profile, IM, with Moho temperature 400 °C and wet olivine mantle. B: Design of the numerical model for stability analysis of lithosphere with a positively buoyant depleted mantle. The temperature at the base of the model (600 km depth), at the base of the lithosphere and at the surface is 1700 °C, 1330 °C and 0 °C, respectively. The arrows represent an example of trajectories of passive markers (after 100 Myr of JS model evolution) to show the convective instabilities developing in sub-lithosphere mantle.

LITHOPROBE project and related studies (Audet and Mareschal, 2004; Burov et al., 1998; Hammer et al., 2010; Lévy and Jaupart, 2011; Lévy et al., 2010; Mareschal and Jaupart, 2004; Kaminski and Jaupart, 2000) have revealed strong lateral heterogeneities in the crustal structure of the Canadian craton. Some of these heterogeneities act as important sub-surface loads, and correspond to large-scale intrusions, ancient crustal mountain roots or lower crustal regions brought to the surface along ancient thrust faults. Others represent lateral trends in crustal density, thermal properties, composition and radiogenic heat production.

As mentioned above, geological constraints reveal steadily flat, almost unaltered topography for the large parts of the Canadian craton, with as little as a few hundred meters of exhumation or burial since the past billion years (Burgess, 2008). For example, despite a depression of 8 km in the Moho, there is almost no topographic imprint of the huge granulitic intrusion in the upper crust of the Kapuskasing area, a fossil low angle thrust bringing deep crustal material up to the surface (Burov et al., 1998). Such "frozen", up to 10 km vertical offsets of Moho boundary at the limits of ancient crustal blocks, with little or no topographic expression, suggest high strength of the Canadian and Australian cratons (Fig. 1B). Noteworthily, only small topographic undulations (<500 m) are observed in the Australian craton, despite the fact that, by contrast to the Canadian craton, it did experience Tertiary compression (Lithgow-Bertelloni and Richards, 1998).

The Canadian and Australian cratons are also known for extensive flexural studies, which provided estimates of the equivalent elastic thickness supporting either the JS rheology model ($T_e$; 70–150 km; Audet and Bürgmann, 2011; Audet and Mareschal, 2004; Forsyth, 1985; Lambeck, 1986; McNutt et al., 1988; Watts, 2001; Kirby and Swain, 2009) or the CB rheology ($T_e$; 10–50 km; McKenzie and Fairhead, 1997).

Finally, even though the data on the Canadian and Australian craton are largely used in this study to build representative "generic" models of the Cratonic lithosphere, it is important to keep in mind that we do not intend to reproduce every particular feature of the Canadian or Australian cratonic shields.

**Table 1**
Model parameters for the three thermo-rheological concepts (JS, IM and CB).

| | | JS model | IM model | CB model |
|---|---|---|---|---|
| T (°C) Moho | | 400 °C | 400 °C | 500 °C |
| Thickness of lithosphere (km) | | 250 | 150 | 150 |
| Crust rheology | Upper | Dry quartz | Dry quartz | Wet quartzite |
| | Lower | Dry diabase | Dry diabase | Dry diabase |
| Lithospheric mantle rheology | | Dry olivine | Wet olivine | Wet olivine |
| Te (km) | | 90 | 45 | 30 |

## 3. Numerical modeling

### 3.1. Numerical approach and model setup

We use the numerical thermo-mechanical modeling approach to assess the mechanical response of the lithosphere in various thermo-rheological contexts. The thermo-mechanically and thermo-dynamically coupled code used here is Flamar v12 (Burov and Yamato, 2008), based on the FLAC-Para(o)voz algorithm; Cundall, 1989; Poliakov et al., 1993). This algorithm is described in detail in the Appendix A and in previous studies (e.g., Burov and Yamato, 2008; Yamato et al., 2008). Here we limit the description to some essential features of the numerical technique.

The code handles (1) free surface boundary condition which is of paramount importance for modeling of topography evolution, (2) large strains, and (3) visco (ductile)-elastic–plastic

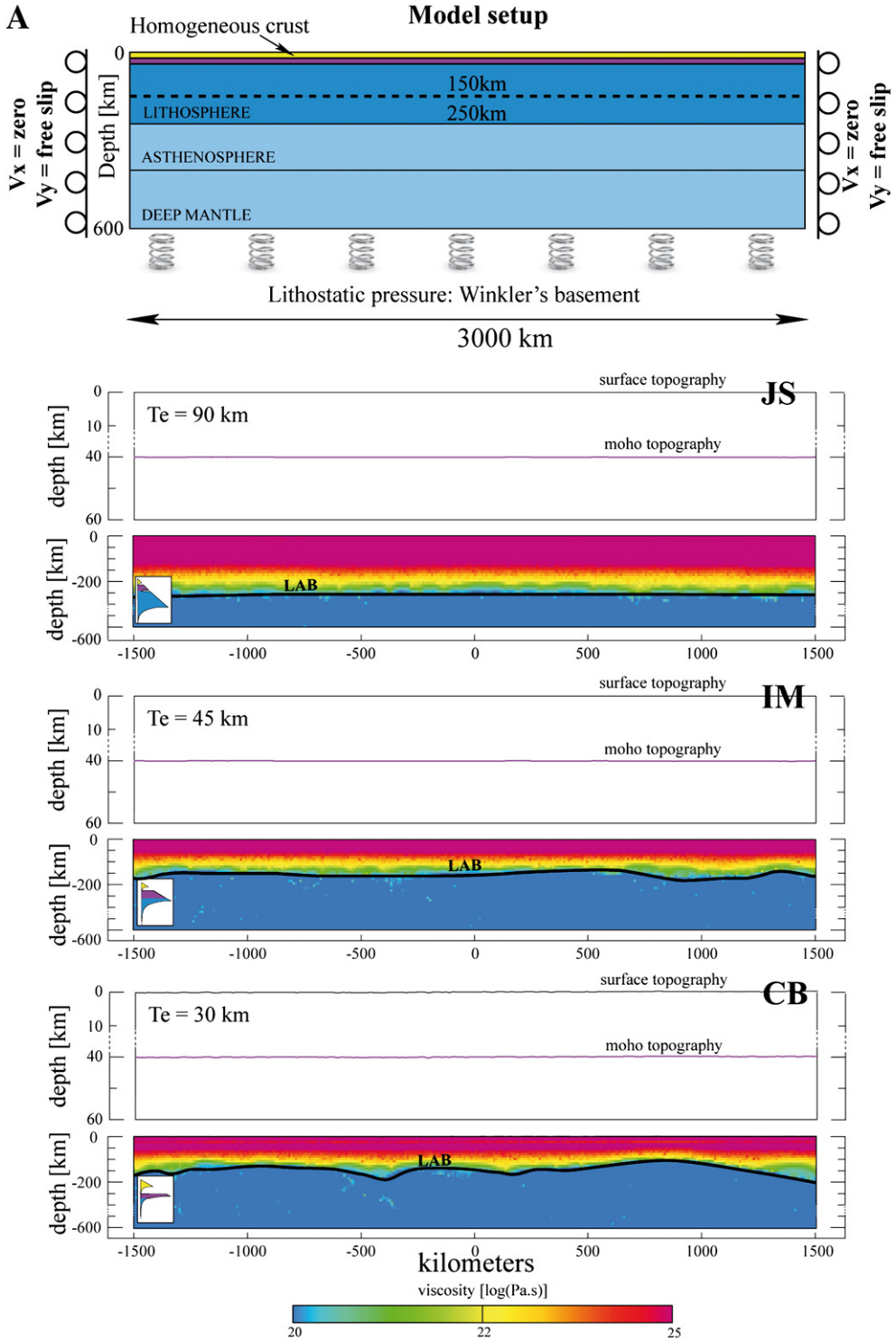


**Fig. 3.** A: Stability tests for semi-infinite cratons with heterogeneous crust, for three rheological assumptions JS, IM and CB, respectively. Geometries of Moho and LAB are shown for each model after 200 Myr. The initial Rayleigh number is approximately $0.7\times10^7$ for JS model, $0.85\times10^7$ for IM model and $10^7$ for CB model (the exact values cannot be defined due to non-linear character of viscosity and compositional density variations). The final Ra numbers do not differ more than by factor of 2 from the initial Ra numbers. Note that in all experiments Moho undulations are very small (not visible at figure scale). B: Time evolution of the surface topography over 200 Myr for the three types of homogeneous semi-infinite craton models shown in panel A.

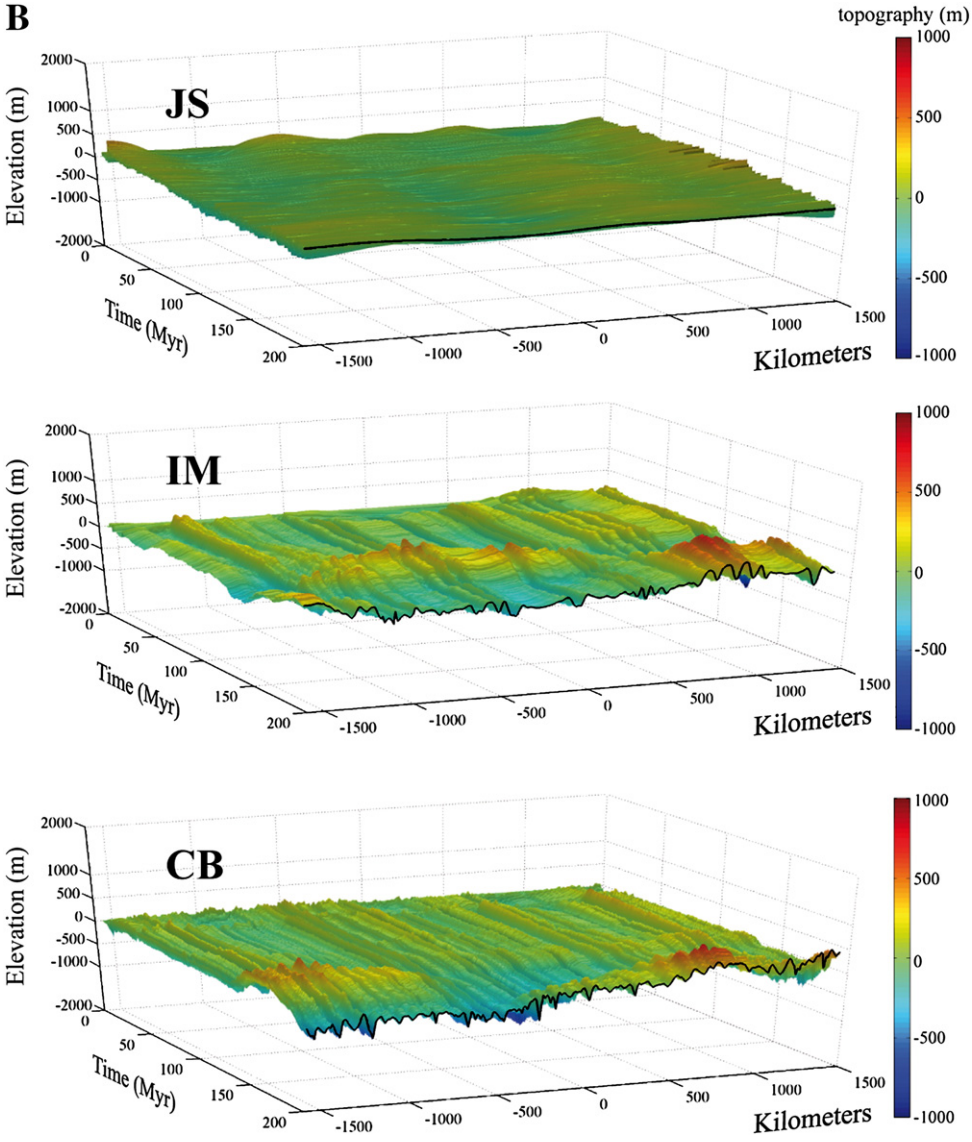


**Fig. 3** (*continued*).

(brittle) rheologies characteristic for different lithospheric and mantle units (see Appendix A). The implemented constitutive laws include linear elasticity, Mohr–Coulomb failure criterion for brittle deformation (faults and thrusting) and pressure–temperature strain-rate dependent ductile flow for viscous deformation. As another key feature, the algorithm takes into account thermo-dynamic phase transitions (Perple_X 2006; Connolly, 2005) and internal heat sources. The code has no intrinsic limitations in treating physical instabilities (see Cundall, 1989) and incorporates particle-in-cell remeshing and tracking of particle trajectories. For the numerical experiments, we use same model setup as shown in Fig. 2B. The multilayered visco-elasto-plastic continental lithosphere is composed of a 40 km-thick free upper-boundary crust, of which the top 20 km upper crustal layer has a dry granite rheology underlain by a 20 km-thick dry diabase lower crust. The total thickness of the lithosphere is 150 km for the CB rheology model, as implied by this thermo-rheological concept (geotherm B, Fig. 1B) and 250 km for the JS rheology model, in accordance with the JS concept (geotherm A, Fig. 1B). The densities are updated dynamically as a function of pressure and temperature (PT) using the thermodynamic free-energy minimization approach (Connolly, 2005). The adopted temperature at the base of the upper mantle is 1700 °C, which corresponds to the assumption of whole mantle convection (Burov and Cloetingh, 2009). The initial thermal gradient in the lithosphere is computed as a function of its age using the half-space cooling model (Burov and Diament, 1995) derived from Parsons and Sclater (1977), which accounts for radiogenic heat sources. The initial temperature at the base of the lithosphere is 1330 °C and the initial linear thermal gradient in the underlying mantle is such that the temperature at 650 km depth is 1700 °C (Schubert et al., 2001). Zero thermal out-flux is used as lateral boundary condition. The mechanical boundary conditions are the following: free upper surface, reflecting boundary conditions or horizontal velocities at the lateral borders, hydrostatically compensated bottom.

In all experiments, the initial "model box" is 3000 km long and 600 km deep with a spatial resolution of 10×10 km. We use the following mechanical boundary conditions: (1) the upper surface is free (free stress and free slip condition in all directions); (2–3) constant horizontal velocity, $v_x$, at the lateral sides ($v_x = 0$ in most experiments); and (4) pliable hydrostatic Winkler basement (Burov et al., 1998). In agreement with the geological record, erosion is considered to be negligible ($k_e = 0$ m$^2$/yr). Thermal initial and boundary conditions vary for the different thermo-rheological scenario considered in this study (Fig 2A, see Appendix A). By contrast to classical studies (Lenardic et al., 2003; Schubert et al., 2001), the Rayleigh number (Ra) of the convective mantle cannot be exactly defined here because

of the non-linear character of the viscosity law and continuous phase changes. Ra varies from approximately $10^7$ to $0.5\times10^6$ in different experiments and through time, so that the upper mantle is highly convective in all our experiments. According to the thermodynamic calculations (Perple_X), the maximum density contrast between a completely depleted Archean mantle and the asthenosphere is on the order of 20–30 kg $m^{-3}$, a value corroborated by independent data on the density of mantle xenoliths (Poudjom Djomani et al., 2001). Since buoyancy favors craton stability, adoption of the maximum value of the density contrast warrants that the thermo-rheological parameters derived from our experiments correspond to the upper-bound stability range.

### 3.2. Numerical experiments

We test the implications of the end-member rheological models (Fig. 2A): "Jelly-Sandwich" rheology (JS; strong dry olivine mantle, strong crust, cold geotherm with Moho temperature of 400 °C, thermal

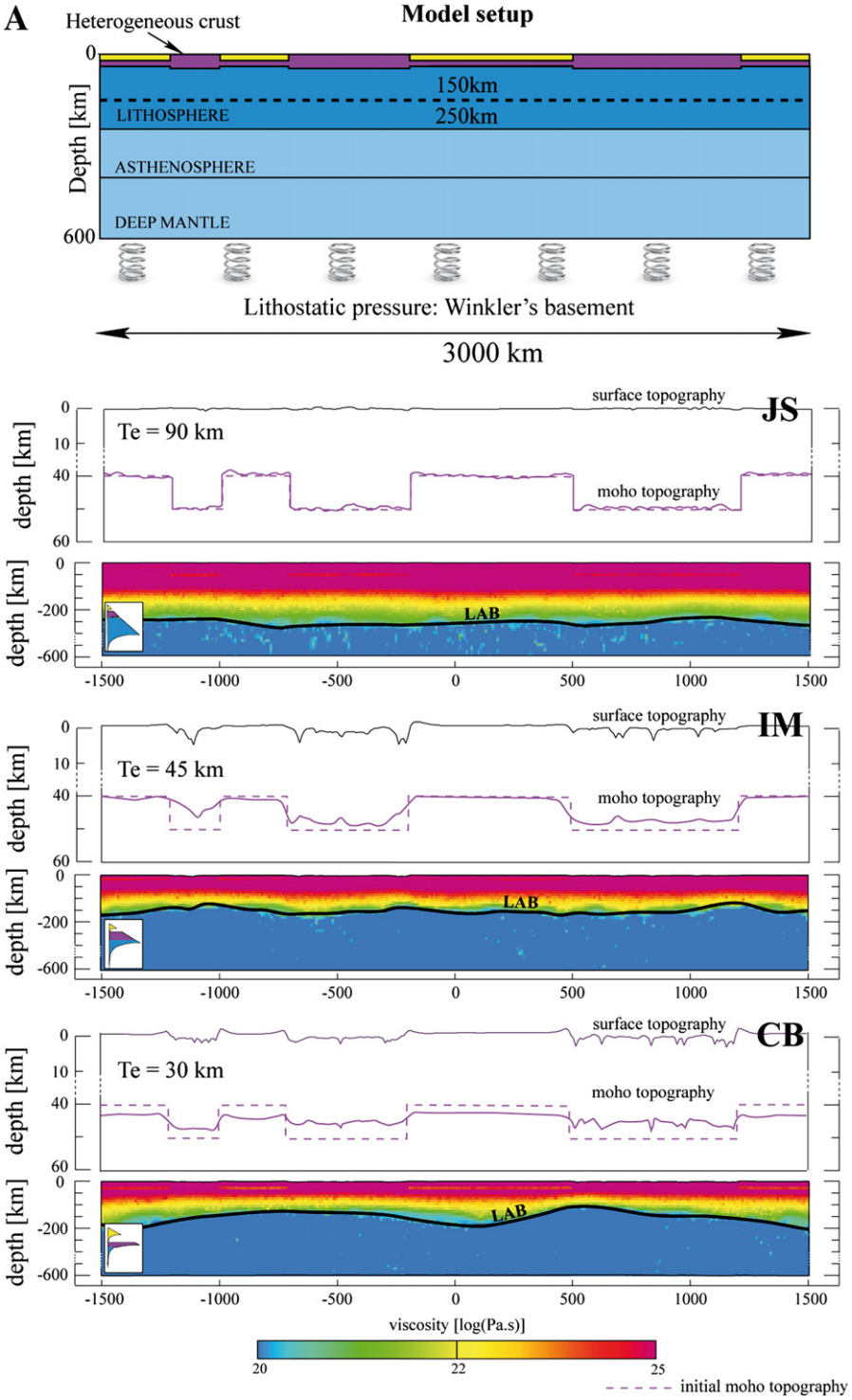


**Fig. 4.** A: Topographic stability tests for semi-infinite cratons with heterogeneous crust, for the three rheological assumptions JS, IM and CB, respectively. Geometries of the surface topography, Moho and LAB are shown for each model after 200 Myr. B: Time evolution of topography over 200 Myr for the three types of heterogeneous semi-infinite craton models shown in panel A.

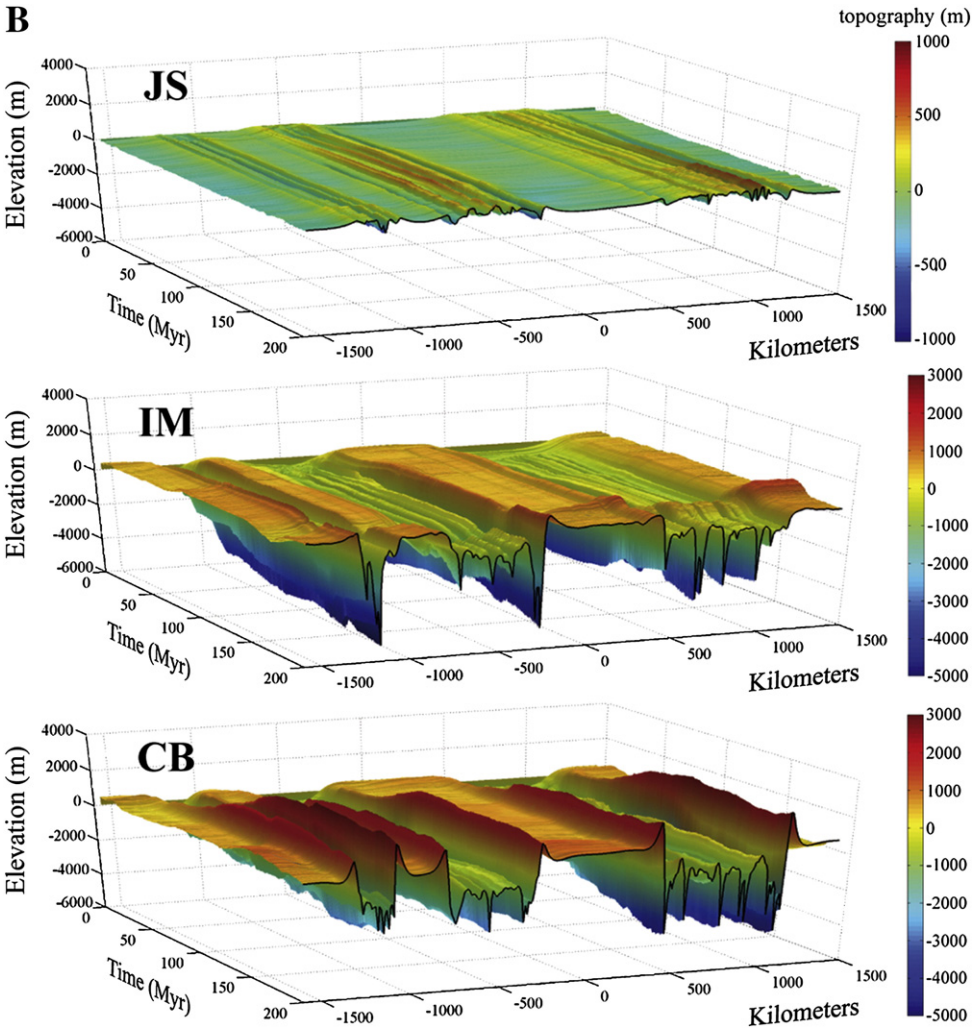


**Fig. 4** (*continued*).

lithosphere thickness of 250 km) and the "Crème Brûlée" rheology (CB; strong dry diabase lower crust, weak wet olivine mantle, Moho temperature of 500 °C, thermal lithosphere thickness of 150 km). We also tested several intermediate rheologies, one of which is represented here by the IM rheology (same rheology parameters and structure as for CB model but cold geotherm as for the JS model) (see Table 1). The JS and IM cases assume the same "cold" initial geotherm based on the latest reconstruction of the thermal structure of the Canadian craton (Cooper and Conrad, 2009). The CB model relies on alternative thermal models based on the assumption of thin "hot" lithosphere (Jackson, 2002; Mackwell et al., 1998; McKenzie and Fairhead, 1997). The rheological impact of the thermal assumptions is crucial and one of the major model sensitivities: the fact that Moho temperature varies from 400 °C to 500 °C between the JS and CB models is all-alone sufficient to produce orders of magnitude differences in the effective viscosity at Moho depths. It is also worth mentioning that for each experiment we also estimated the effective elastic thickness values ($T_e$) following the direct integration method developed in Burov and Diament (1995). This allowed to verify that the $T_e$ of the tested JS model was on the order of 100–110 km matching the upper-bound range observed in cratons. Similarly, $T_e$ of the CB models was on the order of 40–50 km matching the lower bound, admittance-based estimates in cratons.

The first set of experiments shown here (Fig. 3) tests the conditions of the stagnant lid approximation (see Section 2.2 above), that is the stability of a flat layered homogeneous lithosphere structure in the absence of far-field forces. The second set (Figs. 4 and 5) explores the implications of a laterally heterogeneous crustal structure (Fig. 2A), with reference to the Canadian craton. The third set of experiments (Fig. 6) refers to the Australian craton, which, in contrast to the Canadian one, currently undergoes tectonic compression.

Geometrical constraints on crustal thickness and structure for tests 2 and 3 come from the LITHOPROBE project and relevant studies for the Canadian craton (Audet and Mareschal, 2004; Burov et al., 1998; Hammer et al., 2010; Lévy and Jaupart, 2011; Lévy et al., 2010; Mareschal and Jaupart, 2004) and for the Australian craton (Clitheroe et al., 2000; Ford et al., 2010; Stephenson and Lambeck, 1985). In our models we use a statistically representative distribution of crustal heterogeneities with horizontal dimensions in the range of 500–700 km (Fig. 2B; i.e., granulitic bodies that mimic the crustal structure of the Canadian craton: Fig. 1B). The initial Moho geometry is characterized by 10 km vertical steps below the heterogeneities, in line with present-day geophysical observations (Clitheroe et al., 2000; Cook et al., 2010; Hall et al., 2002; Hammer et al., 2010). For the reasons discussed in the previous sections we ran experiments for as long as 750 Myr. This time span is also compatible with that used in most craton stability tests (Beuchert et al., 2010). Even though the Earth system cools down over billions of years, thereby changing the conditions of the mantle convective system, there is no need to run experiments for longer times than 400–700 Myr to test whether the particular configurations will be stable (or not). As we argue below, this time lapse is largely sufficient to discriminate between different thermorheological assumptions, and in fact in most cases the asymptotic behavior of the system becomes clear after

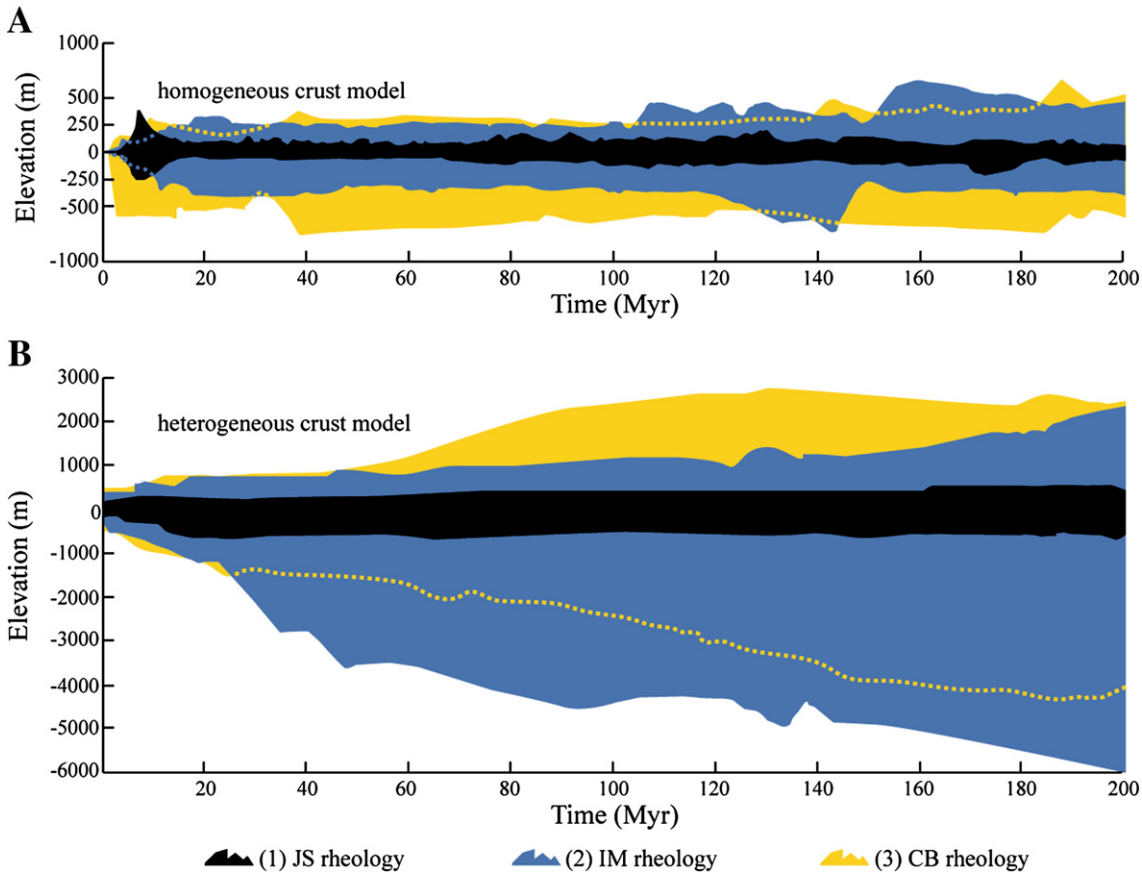


**Fig. 5.** Predicted maximum amplitude of surface topography as a function of time in the case of homogeneous crustal model (A), and heterogeneous crustal model (B), for the three rheological assumptions (JS, IM, CB).

the first 200 Myr. We hence show here the results for 200 Myr snapshots, while the results of longer control experiments are provided in Fig. 7.

### 3.3. Using present-day configuration as initial settings to study cratonic stability

Sleep (2003b) and some other previous studies did consider entrainment of buoyant hot viscous lithosphere and underlying denser mantle with constant properties for a time span of 2 Ga. It hence may be argued that a successful study of cratonic stability should cover their entire lifespan (i.e. 2–2.5 Gyr on average). However, except for simple models, this task is fraught with major uncertainties. Indeed, in their early age cratons were characterized by a hot thermal structure, higher radiogenic heat production and most probably smaller thickness conditioned by poorly constrained convective regimes in early mantle (Michaut et al., 2009). Their rheological properties were also different due to different fluid content and, very likely, composition of their mantle. Finally, during the past 2 Gyr, continents broke and collided a number of times, a process that would be difficult to account for in a single geologically consistent model.

Consequently, our goal is not to reproduce the entire history of Archean cratons but only to constrain the rheology and thermal structure that characterize their present-day state. Indeed, most of the data on cratons come from present-day seismic data, gravity and other geophysical data observations of isostatic balance, and surface heat flow (even if completed by xenolith data that refer to older events). We are also primarily interested in finding constraints on the present day and "recent" properties of cratons to use them as proxy for the rheology of other, more recent continental plates. Observations of topographic evolution in tectonically "quiet" regions are robust enough to conclude that within some cratons there are areas that did not experience significant modifications during the past 500 Myr, or at least that their topography remained stable and did not re-adjust to regain isostatic balance with their heterogeneous crustal structure. On the other hand, such time span, is largely sufficient for thermal relaxation and establishment of a stationary regime in the lithosphere (e.g., Burov and Diament, 1995). In the absence of local thermal events and notwithstanding some decay in radioactive heat production affecting the thermal regime of the crust, the thermal structure of cratons cannot have significantly evolved since the break-up of Gondwana. Consequently, present day conditions in stable cratonic areas must be similar to those prevailing 400–500 Myr ago. Using present-day conditions as initial conditions for our stability models, we therefore test the inferences of different thermo-rheological assumptions for the stability of surface, Moho and LAB topography, so that the successful model should preserve its initial topography and crustal structure within 400–500 Myr. By taking this approach, we can verify if any of the tested thermorheological models (CB, IM or JS) is compatible with the preservation of the inferred crustal and topography structures in Canada and Western Australia.

## 4. Results and discussion

The first "stagnant-lid" experiments (Fig. 3), in which buoyant cratons are expected to be stable for any of the examined rheologies, are used to test the internal consistency of the models. In this case the crust is laterally homogeneous, without imposed far-field tectonic forces and velocities. The computed $T_e$ values at 200 Myr are, respectively, 100–110 km, 60 km, and 40–50 km for JS, IM and CB rheology. They match those typically implied for the corresponding rheologies thus justifying our parameter choices. These experiments show that

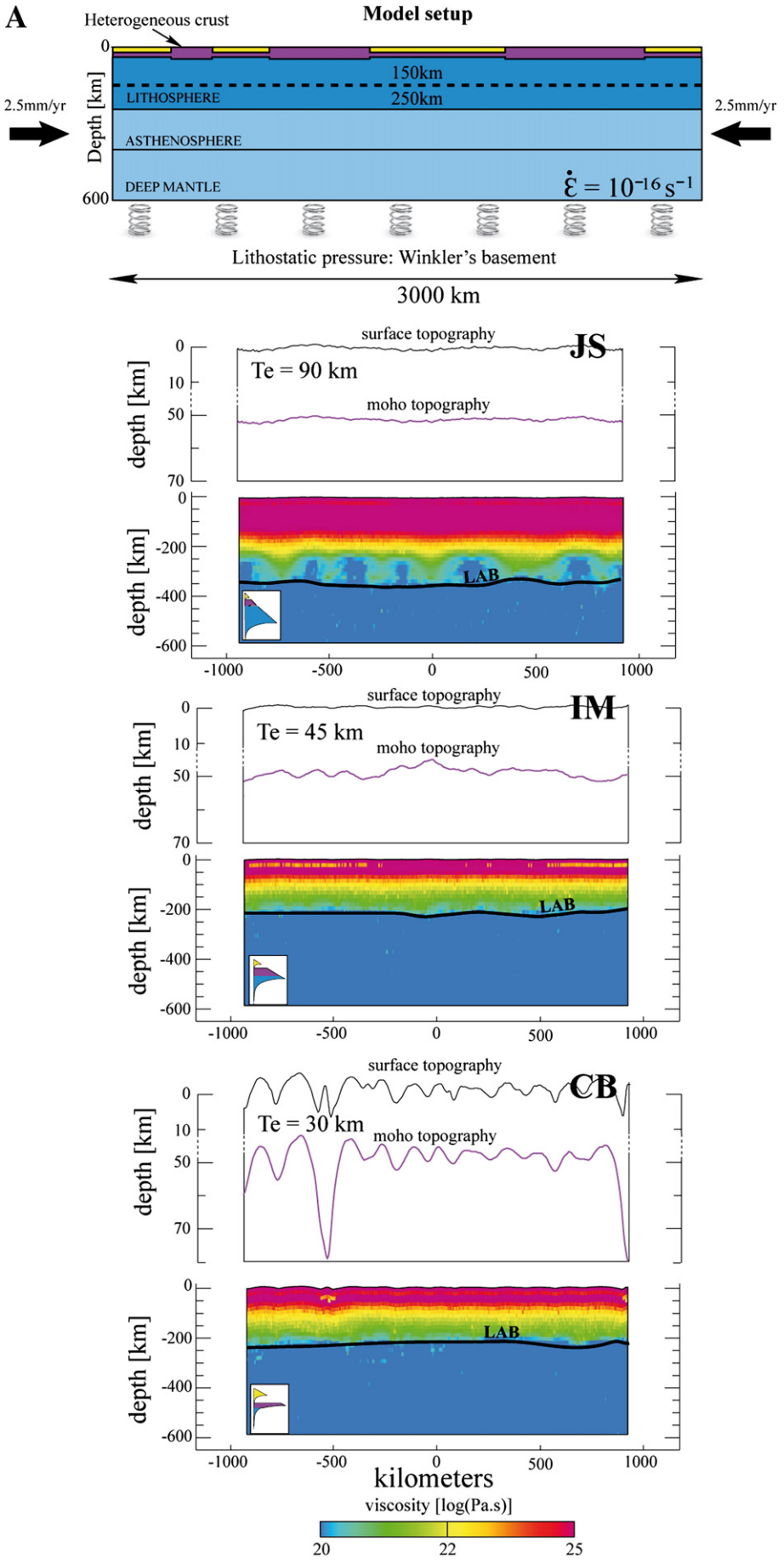
A
Model setup
Heterogeneous crust
0
150km
250km
LITHOSPHERE
ASTHENOSPHERE
DEEP MANTLE
600
Depth [km]
2.5mm/yr
2.5mm/yr
$\dot{\varepsilon} = 10^{-16}\,s^{-1}$
Lithostatic pressure: Winkler's basement
3000 km
surface topography
JS
Te = 90 km
moho topography
depth [km]
LAB
IM
Te = 45 km
CB
Te = 30 km
-1000
-500
0
500
1000
kilometers
viscosity [log(Pa.s)]
20
22
25

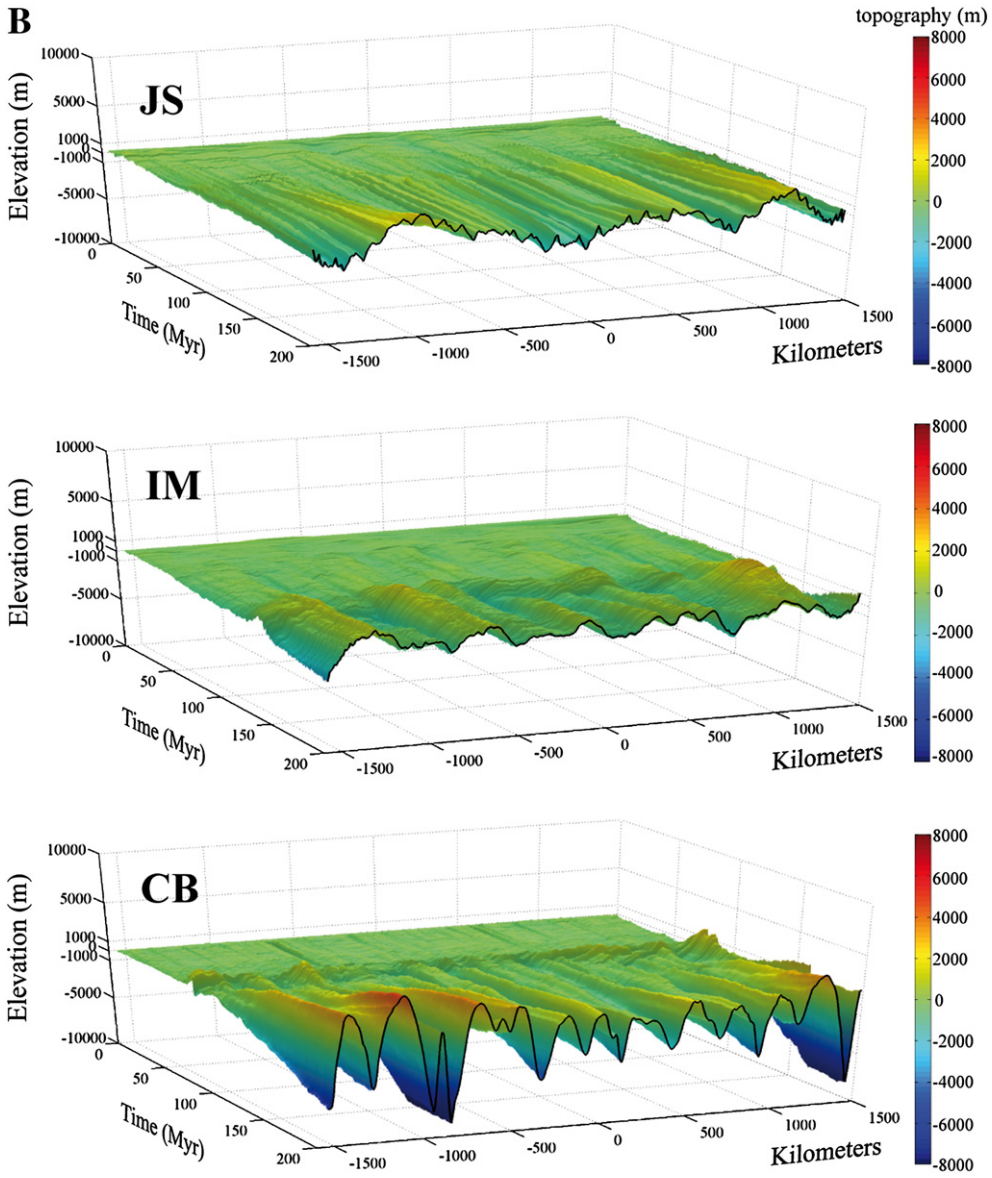


**Fig. 6.** A: Test for semi-infinite cratons with heterogeneous crust and horizontal tectonic forces: Topographic stability tests and time evolution of topography over 200 Myr for semi-infinite cratons with a heterogeneous crust and horizontal tectonic forces (shortening, 5 mm/yr), for the three rheological assumptions JS, IM and CB, respectively. Geometries of the surface topography, Moho and LAB are shown for each model after 200 Myr. B: Time evolution of topography over 200 Myr for the three types of heterogeneous semi-infinite craton models with horizontal tectonic forces shown in panel A.

under the "stagnant lid" conditions the continental lithosphere indeed remains stable (<500 m of surface topography undulations, stable flat Moho) over large time spans (750 Myr), for all tested thermo-rheological assumptions (JS, IM or CB).

By contrast, the second set of experiments, which explores the impact of laterally heterogeneous crust in the absence of far-field tectonic forcing, shows large differences between the three thermo-rheological models (Fig. 4). Surface topography is highly unstable both for the IM and CB rheologies (Fig. 4A) with differences in topographic heights over the borders of crustal heterogeneities on the order of 5000–8000 m (at 200 Myr, Figs. 4B and 5), which are inconsistent with the stratigraphic data on the Canadian and Australian cratons for the corresponding periods of their evolution (Burgess et al., 1997; Gale, 1992; Stephenson and Lambeck, 1985). By contrast, for the JS rheology, the differences in topographic heights do not exceed 200 m (Figs. 4, 5 and 7) and remain within the observed range of topographic roughness. The Moho geometry also shows marked differences between all three models after 200 Myr (Fig. 4B). For the JS model, the initially prescribed 10 km Moho steps are well preserved. For the IM model, the Moho geometry is partly preserved, but locally diverges strongly from the initial geometry. For the CB model, the initial steps in Moho geometry are flattened to only 1–2 km after 200 Myr. The LAB boundary shows a similar trend and is increasingly unstable from the JS to IM and CB rheology. The CB model rapidly exhibits 40–80 km LAB undulations that progressively lead to small-scale convective movements and to removal of a large portion of the mantle lithosphere. For the IM and CB models, the mantle lithosphere is thinned in a number of places by a factor of 1.5–2 by 200 Myr. Given that the growth rate of viscous instabilities is an exponential function of time (e.g., Chandrasekhar, 1961; Houseman et al., 1981), this indicates that 200 Myr interval constitutes the maximum half-life time span of a compositionally positively buoyant CB mantle (Figs. 2 and 4). It is noteworthy that the half-life time of negatively buoyant CB mantle is 5 to 10 times shorter (Burov and Watts, 2006; Houseman et al., 1981), reconfirming the previous idea that compositional buoyancy is a crucial – yet not sufficient – controlling factor in the preservation of cratons (e.g., Burov and Watts, 2006). Since JS experiments did show

practically no modifications in surface and inner structure after the first 200 Myr, we have extended the JS experiments to a 750 Myr duration thus largely exceeding the maximal targeted time span of 500 Myr (Fig. 7). As can be seen, even in this case the lithosphere structure and topography remain stable and practically unchanged compared to its state at 200 Myr.

The comparison between the models involving CB or JS rheology with homogenous or heterogeneous crust shows that the strength of the mantle lithosphere is a major stabilizing factor both for surface topography and subsurface interfaces (i.e., Moho and LAB), while strong crust alone is insufficient to keep topography stable over significant time spans. The experiments without far-field tectonic forces indicate that the buoyancy and strength of the strong mantle lithosphere are both necessary to allow the long-term preservation of cratons. While the previous studies have already shown that lithospheric strength matters for cratonic stability (Guillou-Frottier and Jaupart, 1995; Lenardic et al., 2003; Sleep, 2003b), these experiments show that it is sub-crustal mantle lithosphere and not thick cratonic crust that plays a major role in cratonic stability.

The third set of experiments allows testing the effect of horizontal tectonic forces applied to a cratonic lithosphere. We investigate the impact of a small shortening rate (strain rate $= 10^{-16}$ s$^{-1}$, as for the Australian craton (Celerier et al., 2005)). Although the Australian craton is under compression only since the Tertiary (Lithgow-Bertelloni and Richards, 1998), the numerical experiments allow exploring a longer compression time of 200 Myr (Fig. 6). For the three tested thermo-rheological models, the topographic heights over the first 50 Myr remain within the range of that observed for the Australian craton. Yet, the CB rheology induces unrealistic surface undulations with kilometric topographic heights already at 60 Myr, reaching improbable 12 km heights after 200 Myr. By comparison, the JS and IM rheologies result in more realistic topographic heights of about 4 km after 200 Myr.

Importantly, maximum wavelengths for the 50 and 200 Myr old topography are also more realistic for the JS model (400–700 km that fall in the observed range for the Australian craton) than for the CB model (as small as 100–200 km, i.e. 3–4 times less than observed). The importance of vertical strength partitioning in the lithosphere is another important conclusion that can be derived from these experiments. In fact, high crustal strength alone does not "save" the craton, even for non-negligible integrated lithospheric strength ($T_e = 50$–$60$ km, IM). Strong mantle lithosphere (i.e., $T_e = 100$–$110$ km, JS) is needed to support crustal irregularities and keep surface topography, Moho and LAB stable.

## 5. Conclusions

We herein suggest that testing the stability and evolution of surface topography in thermo-mechanical models of geodynamic processes provides a key tool for constraining mechanical and thermal properties of the lithosphere. We also stress the need to consider buried or "hidden" loads and tectonic forces whenever constraining long-term rheological properties of the Archean lithosphere (and of the lithosphere in general). Our results demonstrate a strong sensitivity of the predicted surface and Moho topographies to thermo-rheological assumptions, thereby allowing for new, stronger constraints on the rheological and thermal structure of cratons and of the continental lithosphere in general.

One of the important results of this study concerns the rheology of the mantle lithosphere and infers that the "Jelly-Sandwich" thermo-rheological model with strong dry olivine mantle, a 250–300 km thick lithosphere and a temperature of 400 °C at Moho depth so far better accounts for geological and geophysical observations in cratons than the "Crème-Brûlée" rheology. Our experiments demonstrate the importance of vertical strength partitioning in the lithosphere by showing that high crustal strength alone is not sufficient for preservation of crustal heterogeneities and long-term stability, even for non-negligible integrated lithospheric strength ($T_e = 50$–$60$ km, IM). Strong mantle lithosphere (i.e., $T_e = 100$–$110$ km, JS) with at least 60–70 km thick strong mechanical layer in the mantle is needed to support crustal irregularities while keeping surface topography, Moho and LAB stable.

The parameter set for dry olivine here (fitting the power flow law with $A = 1 \times 10^4$ MPa$^{-n}$s$^{-1}$, $n = 3$, $Q = 520$ kJ/mol) is, of course, not unique. Based on our experiments and following the approach of Burov and Diament (1995), we can suggest that any other rheological parameter set for the flow law in the lithosphere mantle can be also valid if it is compatible with the prediction of a 60–80 km-thick strong mechanical mantle layer with a steady geotherm passing through 400 °C at 40 km depth and 1330 °C at 250 km depth. The minimal strength of this mechanical layer should be roughly ~5–10 MPa at 800 °C.

We believe that our findings go beyond application to cratons, suggesting, for example, that strong dry olivine mantle lithosphere is universally needed for lithosphere stability and for most lithospheric-scale tectonic processes. In the case of a chemically undepleted mantle ("normal" lithosphere), strong mantle lithosphere, rather than crust, appears to be the main stabilization factor that can ensure the integrity of lithospheric plates within typical time scales of tectonic processes.

## Acknowledgements

We are thankful to N. Sleep, I. Artemieva and the anonymous reviewer for highly constructive comments on the manuscript. This study has been supported by the INSU program SYSTER and partly by ISTEP (UPMC). Thomas François received a Research and Education scholarship granted by UPMC.

## Appendix A. Numerical method, model setup and experiments: extensive description

### A.1. Thermal structure of the lithosphere

The thermal structure is one of the key parameters defining the mechanical strength and buoyancy of the lithosphere. We test three cratonic structures, the "Jelly Sandwich" (JS), the "Intermediate Model" (IM) and the "Crème Brûlée" (CB). The JS geotherm corresponds to commonly inferred cratonic geotherm derived on the basis of surface heat flow measurements, radiogenic heat production data and crustal conductivity data (Lévy et al., 2010; Mareschal and Jaupart, 2004). In this model, the thermal base of the lithosphere (1330 °C) is placed at 250 km depth and surface heat flux is 40 mW m$^{-2}$. For CB thermo-rheological model, we use the geotherm adopted for the CB concept (Mackwell et al., 1998; McKenzie and Fairhead;, 1997). This geotherm is based on upper-bound mantle temperatures derived from mantle xenoliths data (MacKenzie and Canil, 1999) and is equivalent to that used for constructing CB yield-stress envelope for Venus (Mackwell et al., 1998), and for the Earth (Jackson, 2002). According to this model, the thermal base of the lithosphere for CB model is placed at 150 km depth. The surface heat flux is still 40 mW m$^{-2}$ implying fairly higher mantle and near-Moho temperature gradients than in the JS model. Finally the IM model corresponds to the CB rheology with a JS geotherm. We assume zero outflow as a lateral thermal condition on both sides of the box. The initial background geotherm for the mantle–lithosphere system is obtained by joining the lithospheric and deep mantle adiabatic geotherms (approx. 0.3 °C/km (Sleep, 2003b)). Fixed temperatures are used as upper (0 °C) and lower boundary condition (1700 °C at 650 km depth). The initial age-dependent geotherms in the lithosphere are computed according to, Burov and Diament (1992); Burov and Diament (1995) and Parsons and Sclater (1977). For the JS cratonic geotherm, the thermotectonic age yielding the heat flux of 40 mW m$^{-2}$ and 1330 °C at 250 km depth is 500–2000 Ma, which also fits with its geological age. For the "hot" geotherm, the thermal

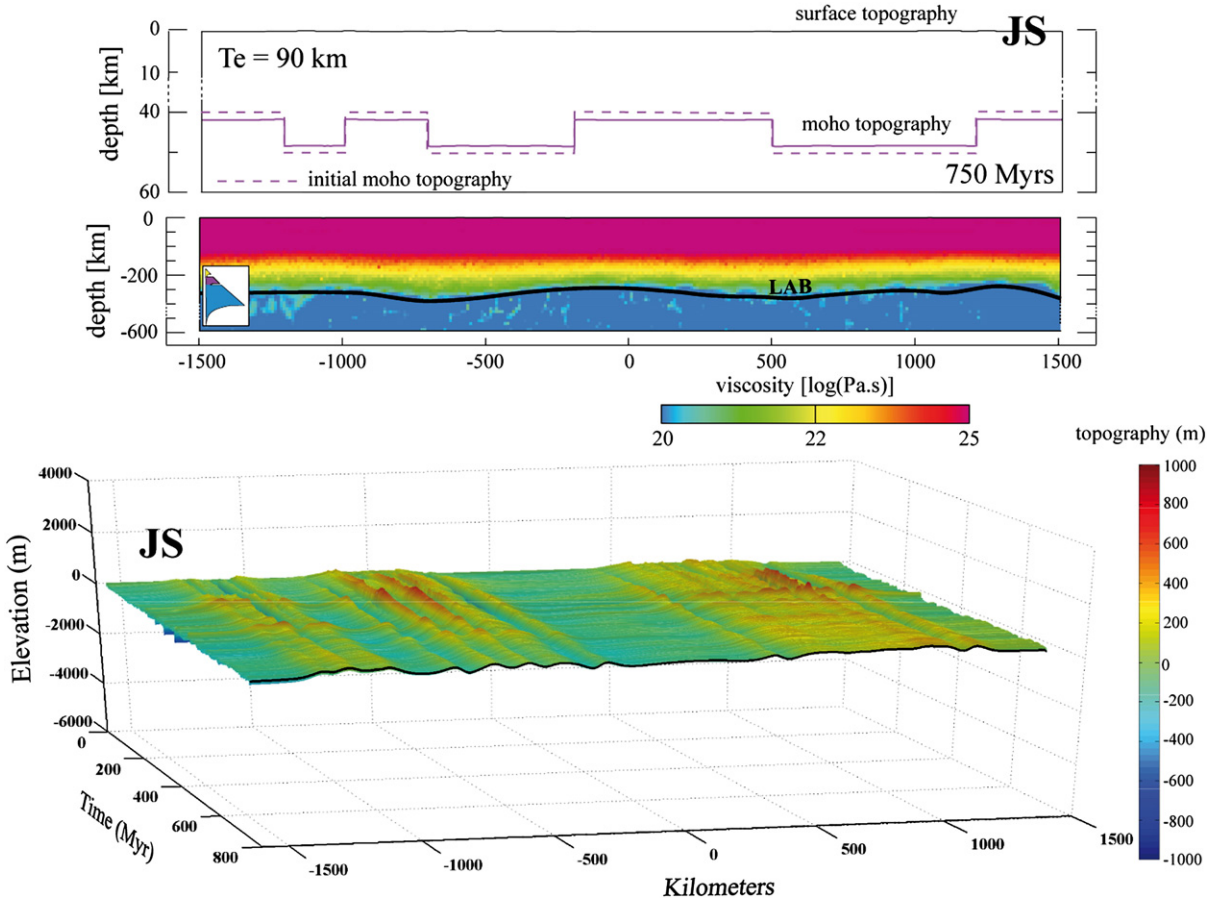


**Fig. 7.** Long time-scale test for semi-infinite cratons with a heterogeneous crust: internal and surface topography evolution over 750 Myr for semi-infinite cratons with heterogeneous crust, for the JS rheological assumption.

age satisfying same boundary condition for surface heat flux and 1330 °C condition at 150 km depth is on the order of 150 Myr. It is impossible to reach stationary state within the time interval corresponding to the geological age of cratons with boundary conditions of the CB model, except if one admits constant heat flux boundary condition at the bottom of the lithosphere (this corresponds to the assumption of small-scale convection in the asthenospheric layer below the lithosphere). However, validation of the thermal model used under the hypothesis of CB rheology is clearly out of the scope of this study.

The initial thermal model for the cold-thick lithosphere model is validated by computing key stagnant parameters that roughly define the thickness of a non-convective layer (lithosphere) overlying convective mantle (Nyblade and Sleep, 2003; Sleep, 2003c; Solomatov, 1995; Solomatov and Moresi, 2000). These parameters are only used to check whether the thermal and rheological parameters used for the lithosphere are roughly compatible with its long-term stability in the absence of external perturbations, i.e. to verify that the lithosphere would form a stable "stagnant lid" on the surface of the convective mantle; the numerical experiments thus start from roughly stable situation. This preliminary analysis is based on the assumption that stagnant lithospheric lid is dominated by heat conduction, in difference from the underlying convective mantle dominated by heat advection. The thickness of this stagnant layer, $Z_{rheo,}$ should be equal to the thickness of mechanically strong lithosphere, i.e. to the thickness of its uppermost portion that is strong enough to prohibit convective flow above its lower boundary thus remaining purely conductive. Hence, $Z_{rheo}$ should be close to the thickness $\delta$ of the conductive lithosphere. The latter equals the sum of thicknesses of the constituent conductive layers, i.e., of the crust ($h_c$~40 km) and of the lithosphere mantle ($h_m = h_l - h_c$):

$$\begin{aligned} d &= h_c + h_m \gg k_m(T_m - T_{moho})/q_m + k_c(T_{moho} - T_0)/q_c \\ &= k(T_m - T_{moho})/q_m + h_c, \end{aligned} \quad (A.1)$$

where $q_m$ is the basal heat flux, $q_c$ is the mean crustal heat flux, $T_m$ is the temperature at the bottom of the stagnant lid, $T_{moho}$ is the temperature at Moho depth $z = h_c$. $q_c$ and $T_{moho}$ are computed from the tested thermal model of the lithosphere, $q_m$, $T_m$, $k$, and $h_c$ are also known. Consequently, $\delta$ can estimated from Eq. (A.1). For JS cratons ($q_m$ = 15–20 mW m$^{-2}$), $\delta$ = 200–250 km (Jaupart et al., 2007). For CB lithosphere $q_m$ = 30 mWt m$^{-2}$, $\delta$ = 120–150 km (Jaupart et al., 2007). $\delta$ only approximately defines the thickness of the stagnant lithosphere $Z_{rheo}$ because the latter also depends on thermally dependent mechanical properties. For these reasons, the next step consists in estimation of the thickness of the rheology boundary layer between the potentially strong upper lid and the underlying weak asthenosphere, and to ensure that the viscosity drop across this layer is compatible with the mechanical stability of the lid. In the stagnant mantle lithosphere, the effective viscosity decreases exponentially as the temperature increases with depth until this process is slowed down by rising pressure and change in the flow law, from dislocation to diffusion creep. The impact of temperature on the viscosity becomes nearly constant in the underlying convecting mantle as the temperature gradient becomes adiabatically small. The depth $Z_{rheo} \leq \delta$ to the zone of transition from a fast viscosity drop (pre-dominant thermal conduction, lithosphere) to nearly constant viscosity (predominant thermal advection, upper mantle) defines the "true" rheological and stagnant thickness of the lithosphere. This zone

**Table A.1**
Thermo-mechanical parameters and boundary conditions used in numerical experiments (Turcotte and Schubert, 2002).

| | | |
|---|---|---|
| Thermal | Surface temperature | 0 °C |
| | Temperature at the bottom of the thermal lithosphere | 1330 °C |
| | Thermal conductivity of crust | 2.5 $Wm^{-1}$ °C |
| | Thermal conductivity of mantle | 3.5 $Wm^{-1}$ °C |
| | Thermal diffusivity of mantle | $10^{-6}$ $m^2$ $s^{-1}$ °C |
| | Radiogenic heat production at surface | $1\times10^{-9}$ W $kg^{-1}$ |
| | Radiogenic heat production decay depth constant | 10 km |
| | Thermo-tectonic age of the lithosphere | 1000 Ma |
| | Surface heat flow | 40 mW $m^{-2}$ |
| | Mantle heat flow | 15 mW $m^{-2}$ |
| Mechanical | Density for all materials | $\rho=f(P,T)$ calculated using Theriak (kg $m^{-3}$) |
| | Lamé elastic constant λ, G (here, λ = G) | 30 GPa |
| | Byerlee's law — friction angle | 30° |
| | Byerlee's law — cohesion | 20 MPa |

is referred to as the rheological boundary layer of thickness $\delta_{rheo}$. This layer separates strong lithosphere ("stagnant lid") from weak underlying mantle and its thickness characterizes the mechanical stability of the "lid". For mantle rheology (Table A.1), the estimated characteristic temperature change for viscosity reduction in the rheology boundary layer is $T_\eta = 50$–65 K. This quantity yields a total temperature change, $T_{rheo}$, across the rheology boundary layer. In our model, $T_{rheo}$, is on the order of 120–150 K (Sleep, 2003a):

$$T_{rheo} \gg 2.4T_h \gg (T_m - T_{moho})/\theta \gg 1/A, \tag{A.2}$$

where $\theta$ is common approximative Frank–Kamenetskii parameter (Solomatov, 1995) defined as $\theta \approx A\Delta T$ where $A$ ($\sim 10^{-2}$ $K^{-1}$) is "activation parameter" for convective flow in the sub-lithosphere mantle (Schubert et al., 2001, p. 618) and $\Delta T = T_m - T_{moho}$. The thickness of the rheological boundary layer, $\delta_{rheo}$ can be estimated as: $\delta_{rheo} \approx T_{rheo}\delta/T_m = 50$ km (Nyblade and Sleep, 2003). Consequently, the characteristic stress scale, $\tau_b \sim (\delta_{rheo} g \rho_m \alpha T_{rheo}) \approx 5$–7 MPa. The value of $\tau_b$ means that if the strength of the lithosphere at its mechanical bottom ($z = Z_{rheo}$) is smaller than $\tau_b$, it may become gravitationally unstable. In this case, the lithosphere thickness will be progressively reduced by a series of mantle drippings that will remove all material which strength is below $\tau_b$. For the geotherms and rheology used, we first checked that the strength of the model cratons is higher than $\tau_b$ down to the depth corresponding to their assumed thickness, which varied from 150 km for CB rheology to 250 km JS rheology. The convective regime in the upper mantle is commonly described by Rayleigh number, Ra which is also uses as a variable parameters of convection models. However, as we also mention in the main text, it is hard or misleading to define a Rayleigh number for a system with strongly varying temperature, strain rate and pressure dependent viscosity, compositionally varying "thermodynamic" density and internal heat sources. This parameter can be estimated only very approximately by depth averaging the properties of the system. This gives us roughly initial Ra of $10^7$ for CB models and $0.7\times10^7$ for JS models. This value changes during the evolution of the system by about factor of 2. Unlike in some previous studies there is no point to vary the general Ra number of the experiments since each time we are testing a concrete situation imposed by already existing thermo-rheological concepts.

## Appendix B. Numerical model

We use our thermo-mechanical code Flamar v12 to assess the response of multilayered visco-elasto-plastic lithosphere. The code is based on the FLAC (Cundall, 1989) and Parovoz algorithm (Poliakov et al., 1993) and is described in many previous studies (e.g., Burov and Cloetingh, 2009; Burov and Guillou-Frottier, 2005; Burov and Poliakov, 2001; Burov et al., 2001, 2003). Here we limit the description of the code to most essential features: the ability to handle (1) large strains and multiple visco-elastic–plastic rheologies (EVP) including Mohr–Coulomb failure (faulting) and non-linear pressure–temperature and strain-rate dependent creep; (2) stain localization; (3) thermo-dynamic phase transitions; (4) internal heat sources; and (5) free surface boundary conditions and surface processes.

### B.1. Basic equations

As its prototypes FLAC (Cundall, 1989) and Parovoz (Poliakov et al., 1993), Flamar has a mixed finite-difference/finite element numerical scheme, with a Cartesian coordinate frame and 2D plane strain formulation. The Lagrangian mesh is composed of quadrilateral elements subdivided into 2 couples of triangular sub-elements with tri-linear shape functions. Flamar uses a large strain fully explicit time-marching scheme. It locally solves full Newtonian equations of motion in a continuum mechanics approximation:

$$\langle \rho \ddot{\mathbf{u}} \rangle - \mathrm{div}\sigma - \rho \mathbf{g} = 0 \tag{B.1}$$

coupled with constitutive equations:

$$\frac{D\sigma}{Dt} = F(\sigma, \mathbf{u}, \dot{\mathbf{u}}, \nabla\dot{\mathbf{u}}, \ldots T \ldots) \tag{B.2}$$

and with equations of heat transfer, with heat advection term $\dot{\mathbf{u}}\nabla T$ included in the Lagrangian derivative D$T$/D$t$, are:

$$\rho C_p DT/Dt - \nabla(k\nabla T) - \sum_i^n H_i = 0 \tag{B.3}$$

$$\rho = f(P,T). \tag{B.4}$$

Here $\mathbf{u}$, $\sigma$, $\mathbf{g}$, and $k$ are the respective terms for displacement, stress, acceleration due to body forces and thermal conductivity. $P$ is pressure (negative for compression). The triangular brackets in Eq. (B.1) specify conditional use of the related term (in quasi-static mode inertial terms are damped using inertial mass scaling (Cundall, 1989). The terms $t$, $\rho$, $C_p$,$T$, and $H_i$ designate respectively time, density, density at reference conditions, specific heat, temperature, internal heat production per unit volume, thermal expansion coefficient and isothermal compressibility. The symbol $\Sigma$ means summation of various heats sources $H_i$. The expression $\rho = f(P,T)$ refers to the formulation, in which phase changes are taken into account and density is computed by a thermodynamic module that evaluates the equilibrium density of constituent mineralogical phases for given $P$ and $T$ as well as latent heat contribution $H_l$ to the term $\sum_i^n H_i \left( \sum_i^n H_i = H_r + H_f + H_l + \ldots \right)$. $\sum_i^n H_i$ also accounts for radiogenic heat $H_r$ and frictional dissipation $H_f$. The terms D$\sigma$/D$t$, $F$ is the objective Jaumann stress time derivative and a functional, respectively. In the Lagrangian method, incremental displacements are added to the grid coordinates allowing the mesh to move and deform with the material. This allows for the solution of large-strain problems while using locally the small-strain formulation: on each time step the solution is obtained in local coordinates, which are then updated in a large-strain mode.

Solution of Eq. (B.1) provides velocities at mesh points used for computation of element strains and of heat advection $\dot{\mathbf{u}}\nabla T$. These strains are used in Eq. (B.2) to calculate element stresses and equivalent forces used to compute velocities for the next time step. Due to the explicit approach, there are no convergence issues, which is rather common for implicit methods in case of non-linear rheologies. The algorithm automatically checks and adopts the internal time step using 0.1–0.5 of Courant's criterion of stability, which warrants stable solution.

### B.2. Phase changes

Direct solution for density (Eq. (B.4), $\rho = f(P,T)$) is obtained from optimization of Gibbs free energy for a typical mineralogical composition (5 main mineralogical constituents) of the mantle and lithosphere. With that goal, we coupled Flamar with the thermodynamic code PERPLE_X (Connolly, 2005). PERPLE_X minimizes free Gibbs energy $G$ for a given chemical composition to calculate an equilibrium mineralogical assemblage for given P–T conditions:

$$G = \sum_{i=1}^{n} \mu N_i \tag{B.5}$$

where $\mu_i$ is the chemical potential and $N_i$ the moles number for each component $i$ constitutive of the assemblage. Given the mineralogical composition, the computation of density is straightforward (Yamato et al., 2007, 2008). The thermodynamic and solid state physics solutions included in PERPLE_X also yield estimations for elastic and thermal properties of the materials, which are integrated in the thermo-mechanical kernel Flamar via Eqs. (B.1), (B.2), (B.3) and (B.4).

### B.3. Explicit elastic–viscous–plastic rheology

We use a serial Maxwell-type solid, in which the total strain increment in each numeric element is defined by a sum of elastic, viscous and brittle strain increments. In contrast to fluid dynamic approaches, where non-viscous rheological terms are simulated using pseudo-plastic and pseudo-elastic viscous terms (e.g., Bercovici et al., 2001; Solomatov and Moresi, 2000), Flamar explicitly treats all rheological terms. The parameters of elastic–ductile–plastic rheology laws for crust and mantle are derived from rock mechanics data (Table B.1) (Kirby and Kronenberg, 1997; Kohlstedt et al., 1995).

### B.4. Plastic (brittle) behavior

The brittle behavior of rocks is described by Byerlee's law (Byerlee, 1978; Ranalli, 1995) which corresponds to a Mohr–Coulomb material with friction angle $\phi = 30°$ and cohesion $|C_0| < 20$ MPa:

$$\tau = C_0 + \sigma_n \tan\phi \tag{B.6}$$

where $\sigma_n$ is normal stress $\sigma_n = 1/3\sigma_I + \sigma_{II}^{dev}\sin\phi$, $1/3\sigma_I = P$ is the effective pressure (negative for compression), $\sigma_{II}^{dev}$ is the second invariant of deviatoric stress, or effective shear stress. The condition of the transition to brittle deformation (function of rupture $f$) reads as: $f = \sigma_{II}^{dev} + P\sin\phi - C_0\cos\phi = 0$ and $\partial f/\partial t = 0$. In terms of principal stresses, the equivalent of the yield criterion (Eq. (B.6)) reads as:

$$\sigma_1 - \sigma_3 = -\sin\phi(\sigma_1 + \sigma_3 - 2C_0/\tan\phi). \tag{B.7}$$

**Table B.1**
Creep parameters used in this study: (1) Ranalli and Murphy (1987); (2) Mackwell et al. (1998); (3) Carter and Tsenn (1987); (4) Wilks and Carter (1990); and (5) Chopra and Paterson (1984).

| | Composition | A | n | ΔG | Ref. |
|---|---|---|---|---|---|
| | | [MPa$^{-n}$ s$^{-1}$] | | [KJ·mol$^{-1}$] | |
| Upper crust | Dry quartzite | $6.8\times10^{-6}$ | 3 | 156 | 1 |
| | Wet quartzite | $1.1\times10^{-4}$ | 4 | 223 | 2 |
| Lower crust | Dry Maryland diabase | $8\pm4$ | $4.7\pm0.6$ | $485\pm30$ | 2 |
| | Dry diabase | $6.3\times10^{-2}$ | 3.05 | 276 | 3 |
| Mantle | Dry olivine | $1\times10^{4}$ | 3 | 520 | 4 |
| | Wet olivine | 417 | 4.48 | 498 | 5 |

### B.5. Elastic behavior

The elastic behavior is described by the linear Hooke's law:

$$\sigma_{ij} = \lambda\varepsilon_{ii}\delta_{ij} + 2G\varepsilon_{ij} \tag{B.8}$$

where λ and G are Lame's constants. Repeating indexes mean summation and δ is the Kronecker's operator.

### B.6. Viscous (ductile) behavior

Within deep lithosphere and underlying mantle regions, creeping flow is highly dependent on temperature and is non-linear non-Newtonian since the effective viscosity also varies as function of differential stress (Kirby and Kronenberg, 1997; Ranalli, 1995):

$$\dot{\varepsilon}^{d} = A(\sigma_1 - \sigma_3)^n \exp\left(-QR^{-1}T^{-1}\right). \tag{B.9}$$

Where $\dot{\varepsilon}^{d}$ is effective shear strain rate, $A$ is a material constant, $n$ is the power-law exponent, $Q = E_a + PV$ is the activation enthalpy, $E_a$ is activation energy, $V$ is activation volume, $P$ is pressure, $R$ is the universal gas constant, $T$ is temperature in K, $\sigma_1$ and $\sigma_3$ are the principal stresses. The effective viscosity $\mu_{eff}$ for this law is defined as:

$$\mu_{eff} = \dot{\varepsilon}^{(1-n)/n} A^{-1/n} \exp\left(Q(nRT)^{-1}\right). \tag{B.10}$$

For non-uniaxial deformation, the law (Eq. (B.10)) is converted to a triaxial form, using the invariant of strain rate and geometrical proportionality factors:

$$\mu_{eff} = \dot{\varepsilon}^{d}{}_{II}{}^{(1-n)/n} (A^*)^{-1/n} \exp\left(Q(nRT)^{-1}\right) \tag{B.11}$$

$$\text{where } \varepsilon^{d}{}_{II} = \left(\text{Inv}_{II}\left(\dot{\varepsilon}_{ij}\right)\right)^{\S} \text{ and } A^* = \S A \cdot 3^{(n+1)/2}.$$

The parameters $A$, $n$, $Q$ are the experimentally determined material constants (Table B.1). Using olivine parameters, we verify that the predicted effective viscosity just below the lithosphere is $10^{19}$–$5\times10^{19}$ Pa s matching post-glacial rebound data (Turcotte and Schubert, 2002). Due to temperature dependence of the effective viscosity, the viscosity decreases from $10^{25}$ to $10^{27}$ Pa s to asthenospheric values of $10^{19}$ Pa s in the depth interval 0–250 km. Within the adiabatic temperature interval in the convective mantle (250 km–650 km), the dislocation flow law (Eq. (B.9)) is replaced by a nearly Newtonian diffusion creep. In this interval, temperature increases very slowly with depth while linearly growing pressure starts to affect viscosity resulting in its slow growth from $10^{19}$ Pa s in the asthenosphere to $10^{21}$ Pa s at the base of the upper mantle (e.g., Turcotte and Schubert, 2002).

## Appendix C. Model setup

The model setup is shown in Fig. 2B. We followed parametric studies by (Burov and Cloetingh, 2009; Burov and Guillou-Frottier, 2005; Burov et al., 2007; d'Acremont et al., 2003) who have modeled mantle–lithosphere interactions for various visco-elasto-plastic lithospheric structures and Rayleigh numbers.

### C.1. Density and thermo-rheological structure

The thermal structure, initial and boundary conditions of the models are described in the beginning of this section. Each element of the numerical grid is assigned its specific material phase defined as a subset of physical parameters of the corresponding material: density, thermal and EVP rheology parameters (Tables A.1 and B.1). All models include a 40 km thick crust and four horizontal rheological layers (Table B.1): (1) a 20 km thick granitic upper crust with mean density

of 2700 kg/m$^3$; (2) a 20 km thick lower crust with an effective rheology defined by JS or CB models and mean density of 2900 kg/m$^3$; (3) a 60 km or 160 km thick olivine mantle lithosphere with density of 3330 kg/m$^3$ at reference temperature; and (4) sub-lithosphere upper mantle with reference density of $\rho_m = 3340$ kg m$^{-3}$, so that the lithosphere is initially gravitationally stable (Ranalli and Murphy, 1987).

### C.2. Mechanical boundary conditions

The mechanical boundary conditions assigned on the four sides of the box are: at the left and right sides: horizontal velocity, $v_x$ (set to zero in most experiments); at the bottom: hydrostatic pressure with free slip in all directions; the upper surface is free (free stress and free slip condition in all directions), without diffusion erosion ($k_e = 0$ m$^2$/yr). The bottom is pliable Winkler basement (= hydrostatic condition).

## References


Artemieva, I.M., 2006. Global 1°×1° thermal model TC1 for the continental lithosphere: implications for lithosphere secular evolution. Tectonophysics 416 (1–4), 245–277.

Artemieva, I.M., 2009. The continental lithosphere: reconciling thermal, seismic, and petrologic data. Lithos 109, 23–46.

Artemieva, I.M., Mooney, W.D., 2001. Thermal thickness and evolution of Precambrian lithosphere: a global study. Journal of Geophysical Research 106 (B6), 16,387–16,414.

Audet, P., Bürgmann, R., 2011. Dominant role of tectonic inheritance in supercontinent cycles. Nature Geoscience 4, 184–187.

Audet, P., Mareschal, J.-C., 2004. Variations in elastic thickness in the Canadian Shield. Earth and Planetary Science Letters 226, 17–31.

Belton, D.X., Brown, R.W., Kohn, B.P., Fink, D., Farley, K.A., 2004. Quantitative resolution of the debate over antiquity of the central Australian landscape: implications for the tectonic and geomorphic stability of cratonic interiors. Earth and Planetary Science Letters 219, 21–34. http://dx.doi.org/10.1016/S0012-821X(03)00705-2.

Bercovici, D., Ricard, Y., Schubert, G., 2001. A two-phase model for compaction and damage. Applications to shear localization and plate boundary formation. Journal of Geophysical Research 106, 8925–8939.

Beuchert, M.J., Podladchikov, Y.Y., Simon, N.S.C., Rüpke, L.H., 2010. Modeling of craton stability using a viscoelastic rheology. Journal of Geophysical Research 115, B11413. http://dx.doi.org/10.1029/2009JB006482.

Bierman, P.R., Caffee, M., 2002. Cosmogenic exposure and erosion history of Australian bedrock landforms. Geological Society of American Bulletin 114, 787–803. http://dx.doi.org/10.1130/0016-7606(2002)114_0787:CEAEHO 2.0.CO;2.

Bird, P., 1979. Continental delamination and the Colorado Plateau. Journal of Geophysical Research 84, 7561–7571.

Bleeker, W., 2003. The late Archean record: a puzzle in ca. 35 pieces. Lithos 71, 99–134.

Burgess, P.M., 2008. Phanerozoic evolution of the sedimentary cover of the North American craton. In: Miall, A.D. (Ed.), The Sedimentary Basins of the United States and Canada. Elsevier, Amsterdam, pp. 31–63.

Burgess, P.M., Gurnis, M., Moresi, L., 1997. Formation of sequences in the cratonic interior of North America by interaction between mantle, eustatic and stratigraphic processes. Geological Society of America Bulletin 108, 1515–1535.

Bürgmann, R., Dresen, G., 2008. Rheology of the lower crust and upper mantle: evidence from rock mechanics, geodesy, and field observations. Annual Review of Earth and Planetary Sciences 36, 531–567. http://dx.doi.org/10.1146/annurev.earth.36.031207.124326.

Burov, E., 2010. The equivalent elastic thickness (Te), seismicity and the long-term rheology of continental lithosphere: time to burn-out "crème brûlée"? Insights from large-scale geodynamic modelling. Tectonophysics 484, 4–26.

Burov, E., 2011. Rheology and strength of the lithosphere. Marine and Petroleum Geology 28 (8), 1402–1443. http://dx.doi.org/10.1016/j.marpetgeo.2011.05.008.

Burov, E., Cloetingh, S., 2009. Controls of mantle plumes and lithospheric folding on modes of intra-plate continental tectonics: differences and similarities. Geophysical Journal International 178, 1691–1722.

Burov, E., Diament, M., 1992. Flexure of the continental lithosphere with multilayered rheology. Geophysical Journal International 109, 449–468.

Burov, E., Diament, M., 1995. Effective elastic thickness of the continental lithosphere — what does it really mean? Journal of Geophysical Research 100, 3905–3927.

Burov, E., Guillou-Frottier, L., 2005. The plume head–continental lithosphere interaction using a tectonically realistic formulation for the lithosphere. Geophysical Journal International 161, 469–490.

Burov, E., Poliakov, A., 2001. Erosion and rheology controls on syn and post-rift evolution: verifying old and new ideas using a fully coupled numerical model. Journal of Geophysical Research 106, 16461–16481.

Burov, E., Watts, A.B., 2006. The long-term strength of continental lithosphere: "jelly-sandwich" or "crème-brulé"? GSA Today 16, 4–10.

Burov, E., Jaupart, C., Mareschal, J.-C., 1998. Large-scale crustal heterogeneities and lithospheric strength in cratons. Earth and Planetary Science Letters 164, 205–219.

Burov, E., Jolivet, L., Le Pourhiet, L., Poliakov, A., 2001. A thermomechanical model of exhumation of HP and UHP methamorphic rocks in Alpine mountain belts. Tectonophysics 342, 113–136.

Burov, E., Jaupart, C., Guillou-Frottier, L., 2003. Emplacement of magma reservoirs in the upper crust. Journal of Geophysical Research 108 (B4), 2177. http://dx.doi.org/10.1029/2002JB001904.

Burov, E., Guillou-Frottier, L., d'Acremont, E., Le Pourhiet, L., Cloetingh, S., 2007. Plume head–lithosphere interactions near intra-continental plate boundaries. Tectonophysics 434, 15–38.

Burov, E., Yamato, P., 2008. Continental plate collision. P-T-t-z conditions and unstable vs. stable plate dynamics: insights from thermo-mechanical modeling. Lithos 103, 178–204.

Byerlee, J.D., 1978. Friction of rocks. Pure and Applied Geophysics 116, 615–626.

Carter, N.L., Tsenn, M.C., 1987. Flow properties of continental lithosphere. Tectonophysics 136, 27–63.

Celerier, J., Sandiford, M., Hansen, D.L., Quigley, M., 2005. Modes of active intraplate deformation, Flinders Ranges, Australia. Tectonics 24. http://dx.doi.org/10.1029/2004&C001679.

Chandrasekhar, S., 1961. Hydrodynamic and Hydromagnetic Stability. Oxford Univ., Oxford. (652pp.).

Chopra, P.N., Paterson, M.S., 1984. The role of water in the deformation of dunite. Journal of Geophysical Research 89 (B9), 7861–7876.

Clitheroe, G., Gudmundsson, O., Kennett, B.L.N., 2000. The crustal thickness of Australia. Journal of Geophysical Research 105, 13,697–13,713.

Connolly, J.A.D., 2005. Computation of phase equilibria by linear programming: a tool for geodynamic modeling and its application to subduction zone decarbonation. Earth and Planetary Science Letters 236, 524–541.

Cook, F.A., White, D.J., Jones, A.G., Eaton, D.W.S., Hall, J., Clowers, R.M., 2010. How the crust meets the mantle: lithoprobe perspectives on the Mohorovicić discontinuity and crust–mantle transition. Canadian Journal of Earth Sciences 47, 315–351. http://dx.doi.org/10.1139/E09-076.

Cooper, C.M., Conrad, C.P., 2009. Does the mantle control the maximum thickness of cratons? Lithosphere 1, 67–72. http://dx.doi.org/10.1130/L40.1.

Cundall, P.A., 1989. Numerical experiments on localization in frictional materials. Archive of Applied Mechanics 59, 148–159.

d'Acremont, E., Leroy, S., Burov, E., 2003. Numerical modelling of a mantle plume: the plume head–lithosphere interaction in the formation of an oceanic large igneous province. Earth and Planetary Science Letters 206, 379–396.

Doin, M.P., Fleitout, L., Christensen, U., 1997. Mantle convection and stability of depleted and undepleted continental lithosphere. Journal of Geophysical Research 102, 2771–2787.

Eaton, D.W., Darbyshire, F., Evans, R.L., Grütter, H., Jones, A.G., Yuan, X., 2009. The elusive lithosphere–asthenosphere boundary (LAB) beneath cratons. Lithos 109, 1–22.

Evans, B., Kohlstedt, D.L., 1995. Rheology of rocks. In: Ahrens, T.J. (Ed.), Rock Physics and Phase Relations: A Handbook of Physical Constants, Ref. Shelf, 3. AGU, Washington, D.C., pp. 148–165.

Ferraccioli, F., Finn, C.A., Jordan, T.A., Bell, R.E., Anderson, L.M., Damaske, D., 2011. East Antarctic rifting triggers uplift of the Gamburtsev Mountains. Nature 479, 388–392.

Fischer, K.M., Ford, H.A., Abt, D.L., Rychert, C.A., 2010. The lithosphere–asthenosphere boundary. Annual Review of Earth and Planetary Sciences 38, 551–575.

Flowers, R.M., Bowring, S.A., Reiners, P.W., 2006. Low long-term erosion rates and extreme continental stability documented by ancient (U–Th)/He dates. Geology 34, 925–928.

Ford, H.A., Fischer, K.M., Abt, D.L., Rychert, C.A., Elkins-Tanton, L.T., 2010. The lithosphere asthenosphere boundary and cratonic lithospheric layering beneath Australia from Sp wave imaging. Earth and Planetary Science Letters 300, 299–310.

Forsyth, D.W., 1985. Subsurface loading and estimates of the flexural rigidity of continental lithosphere. Journal of Geophysical Research 90, 12,623–12,632.

Forte, A.M., Perry, H.K.C., 2000. Geodynamic evidence for a chemically depleted continental tectosphere. Science 290, 1940–1944.

Gale, S., 1992. Long-term landscape evolution in Australia. Earth Surface Processes and Landforms 17, 323–343.

Griffin, W.L., O'Reilly, S.Y., Natapov, L.M., Ryan, C.G., 2003. The origin and evolution of Archean lithospheric mantle. Precambrian Research 127, 19–41.

Guillou-Frottier, L., Jaupart, C., 1995. On the effects of continents on mantle convection. Journal of Geophysical Research 100, 24217–24238.

Gung, Y., Panning, M., Romanowicz, B., 2003. Global anisotropy and the thickness of continents. Nature 422, 707–711.

Gunnell, Y., Fleitout, L., 2000. Morphotectonic evolution of the Western Ghats, India. In: Summerfield, M.A. (Ed.), Geomorphology and Global Tectonics. Wiley, Chichester, pp. 321–338.

Gurnis, M., Mitrovica, J.X., Ritsema, J., Van Heijst, H.-J., 2000. Constraining mantle density structure using geological evidence of surface uplift rates: the case of the African superplume. Geochemistry, Geophysics, Geosystems 1, 1–44.

Hall, J., Keith, E.L., Funck, T., Deemer, S., 2002. Geophysical characteristics of the continental crust along the Lithoprobe Eastern Canadian Shield Onshore–Offshore Transect (ECSOOT): a review. Canadian Journal of Earth Sciences 39, 569–587. http://dx.doi.org/10.1139/E02-005.

Hammer, P.T.C., Clowes, R.M., Cook, F.A., van der Velden, A.J., Vasudevan, K., 2010. The Lithoprobe trans-continental lithospheric cross sections: imaging the internal structure of the North American continent. Canadian Journal of Earth Sciences 47, 821–857.

Houseman, C.A., Molnar, P., 1997. Gravitational (Rayleigh–Taylor) instability of a layer with nonlinear viscosity and convergence thinning of continental lithosphere. Geophysical Journal International 128, 125–150.

Houseman, G.A., McKenzie, D.P., Molnar, P., 1981. Convective instability of a thickened boundary layer and its relevance for the thermal evolution of continental convergent belts. Journal of Geophysical Research 86, 6115–6132.

Jackson, J., 2002. Strength of the continental lithosphere: time to abandon the jelly sandwich? GSA Today 12, 4–10. http://dx.doi.org/10.1130/1052-5173.

Jaupart, C., Mareschal, J.-C., Guillou-Frottier, L., Davaille, A., 1998. Heat flow and thickness of the lithosphere in the Canadian Shield. Journal of Geophysical Research 103, 15269–15288.
Jaupart, C., Labrosse, S., Mareschal, J.-C., 2007. Temperature, heat and energy in the mantle of the Earth. In: Bercovici, D. (Ed.), Treatise on Geophysics. Mantle Dynamics, Vol. 7. Elsevier, Boston, pp. 253–303.
Jordan, T.H., 1981. Continents as a chemical boundary layer. Philosophical Transactions of the Royal Society of London, Series A: Mathematical, Physical and Engineering Sciences 301, 359–373.
Kaminski, E., Jaupart, C., 2000. Lithosphere structure beneath the Phanerozoic intracratonic basins of North America. Earth and Planetary Science Letters 178, 139–149.
Karato, S., 2010. Rheology of the deep upper mantle and its implications for the preservation of the continental roots: a review. Tectonophysics 481, 82–98.
Karato, S., 2012. On the origin of the asthenosphere. Earth and Planetary Science Letters 321–322, 95–103.
Katayama, I., Karato, S.I., Brandon, M., 2005. Evidence for high water content in the deep upper mantle inferred from deformation microstructures. Geology 33 (7), 613–616.
Keefner, J.W., Mackwell, S.J., Kohlstedt, D.L., Heidelbach, F., 2011. Dependence of dislocation creep of dunite on oxygen fugacity: implications for viscosity variations in Earth's mantle. Journal of Geophysical Research 116. http://dx.doi.org/10.1029/2010JB007748.
Kirby, S.H., Kronenberg, A.K., 1997. Rheology of the lithosphere: selected topics. Reviews of Geophysics 25, 1219–1244.
Kirby, J.F., Swain, C.J., 2009. A reassessment of spectral Te estimation in continental interiors: the case of North America. Journal of Geophysical Research 114. http://dx.doi.org/10.1029/2009JB006356.
Kohlstedt, D.L., Evans, B., Mackwell, S.J., 1995. Strength of the lithosphere: constraints imposed by laboratory experiments. Journal of Geophysical Research 100, 17 587–17 602.
Kopylova, M.G., Russell, J.K., 2000. Chemical stratification of cratonic lithosphere: constraints from the Northern Slave craton, Canada. Earth and Planetary Science Letters 181, 71–87.
Kopylova, M.G., Russell, J.K., Cookenboo, H., 1999. Petrology of peridotite and pyroxenite xenoliths from the Jericho kimberlite: implications for thermal state of the mantle beneath the Slave craton, northern Canada. Journal of Petrology 40-1, 79–104.
Korenaga, J., Jordan, T.H., 2002. On the state of sublithospheric upper mantle beneath a supercontinent. Geophysical Journal International 149, 179–189. http://dx.doi.org/10.1046/j.1365-246X.2002.01633.x.
Lambeck, K., 1986. Crustal structure and evolution of the central Australian basins. In: Dawson, J.B., Carswell, D.A., Hall, J., Wedepohl, K.H. (Eds.), The Nature of the Lower Continental Crust, Geological Society, London, pp. 113–145. Special publication No. 24.
Lenardic, A., Moresi, L.N., Mühlhaus, H., 2003. Longevity and stability of cratonic lithosphere: insights from numerical simulations of coupled mantle convection and continental tectonics. Journal of Geophysical Research, B: Solid Earth and Planets 108 (B6), 2303. http://dx.doi.org/10.1029/2002JB001859.
Lévy, F., Jaupart, C., 2011. Temperature and rheological properties of the mantle beneath the North American craton from an analysis of heat flux and seismic data. Journal of Geophysical Research 116, B01408. http://dx.doi.org/10.1029/2010JB007726.
Lévy, F., Jaupart, C., Mareschal, J.-C., Bienfait, G., Limare, A., 2010. Low heat flux and large variations of lithospheric thickness in the Canadian Shield. Journal of Geophysical Research 115, B06404. http://dx.doi.org/10.1029/2009JB006470.
Lithgow-Bertelloni, C., Richards, M.A., 1998. The dynamics of Cenozoic and Mesozoic plate motions. Reviews of Geophysics 36, 27–78.
MacKenzie, J.M., Canil, D., 1999. Composition and thermal evolution of cratonic mantle beneath the central Archean Slave Province, NWT, Canada. Contributions to Mineralogy and Petrology 134, 313–324.
Mackwell, S.J., Zimmerman, M.E., Kohlstedt, D.L., 1998. High-temperature déformation of dry diabase with applications to tectonics on Venus. Journal of Geophysical Research 103, 975–984. http://dx.doi.org/10.1029/97JB02671.
Mareschal, J.-C., Jaupart, C., 2004. Variations of surface heat flow and lithospheric thermal structure beneath the North American craton. Earth and Planetary Science Letters 223, 65–77.
McKenzie, D.P., Fairhead, J.D., 1997. Estimates of the effective elastic thickness of the continental lithosphere from Bouguer and free-air gravity anomalies. Journal of Geophysical Research 102, 27523–27552.
McNutt, M.K., Diament, M., Kogan, M.G., 1988. Variation of elastic plate thickness at continental thrust belts. Journal of Geophysical Research 93 (B8), 8825.
Michaut, C., Jaupart, C., Mareschal, J.C., 2009. Thermal evolution of cratonic roots. Lithos 109, 47–60. http://dx.doi.org/10.1016/j.lithos.2008.05.008.
Nyblade, A.A., Sleep, N.H., 2003. Long lasting epeirogenic uplift from mantle plumes and the origin of the Southern African Plateau. Geochemistry, Geophysics, Geosystems 4 (2003GC000573).
Parsons, B., Sclater, G.S., 1977. An analysis of the variation of ocean floor bathymetry and heat flow with age. Journal of Geophysical Research 82, 803–827.
Pillans, B., 2007. Pre-Quaternary landscape inheritance in Australia. Journal of Quaternary Science 22, 439–447.
Poliakov, A.N.B., Cundall, P., Podladchilov, Y., Laykhovsky, V., 1993. An explicit inertial method for the simulation of visco-elastic flow: an evaluation of elastic effects on diapiric flow in two or three-layer models. In: Stone, D.B., Runcorn, S.K. (Eds.), Flow and Creep in The Solar System: Observations, Modelling and Theory: Dynamic Modelling and Flow in the Earth Planet Series, pp. 175–195.
Poudjom Djomani, Y.H., O'Reilly, S.Y., Griffin, W.L., Morgan, P., 2001. The density structure of subcontinental lithosphere through time. Earth and Planetary Science Letters 184, 605–621.
Pysklywec, R.N., Beaumont, C., Fullsack, P., 2000. Modeling the behavior of the continental mantle lithosphere during plate convergence. Geology 28, 655–659.
Ranalli, G., 1995. Rheology of the Earth2nd edn. Chapman and Hall, London. (413pp.).
Ranalli, G., Murphy, D.C., 1987. Rheological stratification of the lithosphere. Tectonophysics 132, 281–295.
Rowland, A., Davies, J.H., 1999. Buoyancy rather than rheology controls the thickness of the overriding mechanical lithosphere at subduction zones. Geophysical Research Letters 26, 3037–3040.
Schubert, G., Turcotte, D.L., Olson, P., 2001. Mantle Convection in the Earth and Planets. Cambridge Univ. Press, Cambridge, U.K. (956pp.).
Shapiro, S.S., Hager, B.H., Jordan, T.H., 1999. Stability and dynamics of the continental tectosphere. Lithos 48, 115–133.
Shapiro, N.M., Ritzwoller, M.H., 2002. Monte Carlo inversion for a global shear velocity model of the crust and upper mantle. Geophysical Journal International 151, 88–105.
Sleep, N.H., 2003a. Geodynamic implications of xenolith geotherms. Geochemistry, Geophysics, Geosystems 4 (9), 1079. http://dx.doi.org/10.1029/2003GC000511.
Sleep, N.H., 2003b. Survival of Archean cratonal lithosphere. Journal of Geophysical Research 108, 2302. http://dx.doi.org/10.1029/2001jb000169.
Sleep, N.H., 2003c. Fate of mantle plume material trapped within a lithospheric catchment with reference to Brazil. Geochemistry, Geophysics, Geosystems 4 (7), 8509. http://dx.doi.org/10.1029/2002GC000464.
Solomatov, V.S., 1995. Scaling of temperature- and stress-dependent viscosity convection. Physics of Fluids 7, 266–274.
Solomatov, V.S., Moresi, L.N., 1997. Three regimes of mantle convection with non-Newtonian viscosity and stagnant lid convection on the terrestrial planets. Geophysical Research Letters 24, 1907–1910.
Solomatov, V.S., Moresi, L.N., 2000. Scaling of time-dependent stagnant lid convection; application to small-scale convection on Earth and other terrestrial planets. Journal of Geophysical Research 105, 21795–21817.
Stephenson, R.A., Lambeck, K., 1985. Isostatic response of the lithosphere with in-plane stress: application to Central Australia. Journal of Geophysical Research 90, 8581–8588.
Stewart, A.J., Blake, D.H., Ollier, C.D., 1986. Cambrian river terraces and ridgetops in central Australia: oldest persisting landforms? Science 233, 758–761.
Tao, W.C., O'Connell, R.J., 1992. Ablative subduction: a two-sided alternative to the conventional subduction model. Journal of Geophysical Research 97, 8877–8904.
Turcotte, D.L., Schubert, G., 2002. Geodynamics, Applications of Continuum Physics to Geological Problems2nd edn. Cambridge Univ. Press, Cambridge.
Watts, A.B., 2001. Isostasy and Flexure of the Lithosphere. Cambridge University Press, Cambridge. (458pp.).
Watts, A.B., Burov, E.B., 2003. Lithospheric strength and its relationship to the elastic and seismogenic thickness. Earth and Planetary Science Letters 213, 113–131.
Wilks, K.R., Carter, N.L., 1990. Rheology of some continental lower crust. Tectonophysics 182, 55–77.
Willet, S., Beaumont, C., Fullsack, P., 1993. Mechanical model for the tectonics of doubly vergent compressional orogens. Geology 21, 371–374.
Xu, Y.G., 2001. Thermo-tectonic destruction of the Archean lithospheric keel beneath the Sino-Korean Craton in China: evidence, timing and mechanism. Physics and Chemistry of the Earth 26, 747–757.
Yamato, P., Agard, P., Burov, E., Le Pourhiet, L., Jolivet, L., Tiberi, C., 2007. Burial and exhumation in a subduction wedge: mutual constraints from thermomechanical modeling and natural P–T–t data (Schistes Lustrés, western Alps). Journal of Geophysical Research 112.
Yamato, P., Burov, E., Agard, P., Le Pourhiet, L., Jolivet, L., 2008. HP–UHP exhumation processes during continental subduction (W. Alps): when thermomechanical models reproduce P–T–t data. Earth and Planetary Science Letters 271, 63–75.